1-31-2009

Variations of Ice Bed Coupling Beneath and Beyond Ice Streams: The Force Balance

Terence J. Hughes
University of Maine - Main, terry.hughes@maine.edu

Variations of ice bed coupling beneath and beyond ice streams: The force balance

T. Hughes[1]

Received 24 March 2008; revised 18 August 2008; accepted 10 October 2008; published 31 January 2009.

[1] A geometrical force balance that links stresses to ice bed coupling along a flow band of an ice sheet was developed in 1988 for longitudinal tension in ice streams and published 4 years later. It remains a work in progress. Now gravitational forces balanced by forces producing tensile, compressive, basal shear, and side shear stresses are all linked to ice bed coupling by the floating fraction φ of ice that produces the concave surface of ice streams. These lead inexorably to a simple formula showing how φ varies along these flow bands where surface and bed topography are known: $\varphi = h_O/h_I$ with h_O being ice thickness h_I at $x = 0$ for x horizontal and positive upslope from grounded ice margins. This captures the basic fact in glaciology: the height of ice depends on how strongly ice couples to the bed. It shows how far a high convex ice sheet ($\varphi = 0$) has gone in collapsing into a low flat ice shelf ($\varphi = 1$). Here φ captures ice bed coupling under an ice stream and h_O captures ice bed coupling beyond ice streams.

Citation: Hughes, T. (2009), Variations of ice bed coupling beneath and beyond ice streams: The force balance, *J. Geophys. Res.*, *114*, B01410, doi:10.1029/2008JB005714.

1. Introduction

[2] Ice sheets, past and present, consist of slow sheet flow from interior ice domes over some 90% of the glaciated area, but up to 90% of sheet flow converges into fast ice streams which end as ice lobes on land or ice tongues in water. Within confining embayments, ice tongues can merge to form broad floating ice shelves that are often grounded locally. Initial attempts at ice sheet modeling dealt with only sheet flow and employed the shallow ice approximation in which the local gravitational driving stress was balanced only by the local basal shear stress. This restriction gave these models a slow passive response to changes in Earth's climate. Landmark work of this kind began with the two-dimensional thermomechanical steady state flow band model by *Budd et al.* [1971] and has led to the three-dimensional thermomechanical time-dependent grid point model by *Huybrechts* [1990], with both models applied to the Antarctic Ice Sheet. These models proliferated and even generated fast currents of ice akin to ice streams through the mass balance but not from the force balance. They gained wide acceptance.

[3] The shallow ice approximation would not allow these models to generate the rapid changes in size and shape demanded by the geological record and linked to the rapid changes in climate recorded in ice sheet core holes, notable the GRIP and GISP 2 core holes to bedrock through the central dome of the Greenland Ice Sheet [e.g., *Mayewski et al.*, 1997]. Holistic models were needed that provided a dynamic thermomechanical link between sheet flow, stream flow, and shelf flow, such that minor changes at local boundaries would affect the stability of the entire ice sheet. This goal has now become the major focus of ice sheet modeling. Far-field processes affect the local force balance through longitudinal force gradients, not through local shear stresses. These gradients are linked to the longitudinal tensile stress, which may be minor locally compared to the basal shear stress. Yet minor perturbations in the force balance of fringing ice shelves can propagate far up ice streams into the heart of an ice sheet, as *Thomas* [2004] showed for Jakobshavn Isbrae in Greenland and *Thomas et al.* [2004] and *Dupont and Alley* [2005, 2006] showed for Pine Island Glacier in Antarctica.

[4] Solutions for flow in standard ice sheet numerical models are obtained by integrating the equilibrium equations $\partial\sigma_{ij}/\partial j + \rho g_i = 0$ which relate stress gradients $\partial\sigma_{ij}/\partial j$ to density ρ and gravity acceleration g_i. Subscripts i and j refer to axes x, y, z in standard tensor notation. None of the stresses σ_{ij} calculated in this way is linked directly to the floating fraction of ice, and therefore to ice bed coupling under ice streams. A full-stress solution providing this linkage is needed in thermomechanical ice sheet models. For examples of progress in this direction, see *MacAyeal* [1989], *Johnson and Fastook* [2002], *Pattyn* [2002], *Hindmarsh* [2004], *Marshall* [2005], and *Schoof* [2007]. Here it is shown how the linkage can be provided geometrically for the most important stresses in ice streams, with the link being the floating fraction of ice for all stresses.

[5] As originally defined by *Bader* [1961] (quoted by *Hughes* [1998 p. 166]),

> An 'ice stream' is something akin to a mountain glacier consisting of a broad accumulation basin and a narrower valley glacier, but a mountain glacier is laterally hemmed in by rock

[1]Department of Earth Sciences, Climate Change Institute, University of Maine, Orono, Maine, USA.

0148-0227/09/2008JB005714$09.00

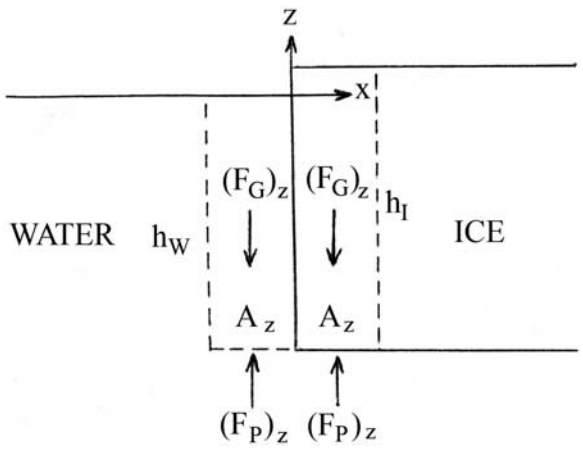

Figure 1. The vertical force balance at the calving front of an ice shelf. Water (left) and ice (right) columns have identical basal areas A_z and respective heights h_W and h_I. Gravity forces $(F_G)_z$ are balanced by pressure forces $(F_P)_z$ with basal pressures $P_W = P_I$ for water and ice.

slopes, while the ice stream is contained by slower moving surrounding ice. The edges of the ice stream are often crevassed, and the surface tends to be concave as the ice is 'funneled' down. Many of the large outlet glaciers in Greenland, particularly in the south, are the narrow outlets of large ice streams which reach back many scores of miles into the ice sheet.

[6] This definition identifies two characteristics of ice streams. (1) Their fast gravitational motion produces a downdrawn concave surface profile. (2) Fast streamflow is resisted by a longitudinal tensile stress that downdraws ice, a side shear stress between fast streamflow and the flanking slow sheet flow, and a basal shear stress that resists slow sheet flow and, although reduced under ice streams, resists fast stream flow.

[7] Section 2 shows that the concave surface of ice streams is caused by a decrease in floating fraction φ of ice upslope from the grounded marine margin of an ice sheet flow band. Section 3 shows how longitudinal tensile and compressive stresses σ_T and σ_C and basal and side shear stresses τ_O and τ_S vary with φ along the flow band. Section 4 presents three applications of the force balance to ice sheet flow bands, two compare flow band profiles from the force balance with profiles that also include the mass balance, and one calculates φ variations in the force balance along Antarctic flow lines that enter major ice streams. Section 5 presents the main conclusions from using the geometrical approach to the force balance and discusses strengths and weaknesses of this approach. Appendix A presents geometrical derivations giving the dependence of ice stream stresses on φ.

2. Producing the Concave Profile of Ice Streams

[8] The concave surface of streamflow connects the low flat surface of fully floating shelf flow to the high convex surface of fully grounded sheet flow. Hence, streamflow represents a transition from sheet flow to shelf flow caused by progressive downstream ice bed uncoupling. Tensile stress σ_T associated with the downdrawn concave surface of an ice stream is obtained by combining the vertical and horizontal force balance. Take x horizontal and positive upstream, y horizontal transverse to flow, and z vertical and positive upward. For marine ice streams, the origin of coordinates is at the grounding line joining shelf flow to stream flow, midway across the ice stream, and at sea level. In the usual tensor notation, for which indices i, j denote axes x, y, z, applied stresses σ_{ij} are related to deviator stresses σ'_{ij} through confining pressure P as follows:

$$\sigma_{ij} = \sigma'_{ij} + \delta_{ij} P \tag{1}$$

where δ_{ij} is the Kronecker delta ($\delta_{ij} = 1$ when $i = j$ and $\delta_{ij} = 0$ when $i \neq j$) and stresses σ'_{ij} are related to strain rates $\dot{\varepsilon}_{ij}$ that produce the downdrawn concave surface of an ice stream.

[9] As illustrated in Figure 1 at the calving front of an ice shelf, confining pressures P of ice or water are determined almost entirely by vertical overburden stress σ_{zz} so that $P = 1/3(\sigma_{xx} + \sigma_{yy} + \sigma_{zz}) \approx \sigma_{zz}$ and the effects of flow on P can be ignored in a vertical force balance. Then Newton's second and third laws of motion give gravitational force $(F_G)_z = \rho g h A_z$ for density ρ through height h above basal area A_z and $(F_G)_z$ is opposed by basal pressure force $(F_P)_z = PA_z$ for both ice and water. Taking ρ_I, h_I, and P_I for ice and ρ_W, h_W, and P_W for water in incremental flow band area $A_z = w_I \Delta x$ for width w_I and length Δx:

$$P_I = \rho_I g h_I \tag{2}$$

$$P_W = \rho_W g h_W \tag{3}$$

where buoyancy requires that $P_I = P_W$ at the base of floating ice.

[10] An expression for longitudinal tensile stress σ_T averaged through h_I is produced by a horizontal force balance in direction x opposite ice flow. Following *Thomas* [1973a, 1973b], linear shelf flow is resisted by σ_T, which is related to σ'_{xx} averaged through h_I as follows. Ignoring compaction of surface snow, σ_{xx}, σ_{yy}, and σ_{zz} become linearly more compressive with depth. For extending streamflow along x, σ_{xx} is slightly less compressive than σ_{zz} so that applying equation (1) gives the defining expression for tensile stress σ_T averaged through the ice thickness, taking $P = \bar{P}_I$ for ice pressure averaged through h_I:

$$\begin{aligned}\sigma_T &= \sigma_{xx} - \sigma_{zz} = \left(\sigma'_{xx} + \bar{P}_I\right) - \left(\sigma'_{zz} + \bar{P}_I\right) = \sigma'_{xx} - \sigma'_{zz} \\ &= \sigma'_{xx} + \left(\sigma'_{xx} + \sigma'_{yy}\right) = \left(2 + \sigma'_{yy}/\sigma'_{xx}\right)\sigma'_{xx} = \left(2 + \dot{\varepsilon}_{yy}/\dot{\varepsilon}_{xx}\right)\sigma'_{xx}\end{aligned} \tag{4}$$

where σ_T is caused by vertical strain rate $\dot{\varepsilon}_{zz}$ due to gravitational thinning, $\dot{\varepsilon}_{xx}$ and $\dot{\varepsilon}_{yy}$ are longitudinal and transverse strain rates, respectively linked to σ'_{xx} and σ'_{yy}, and $\sigma'_{xx} + \sigma'_{yy} + \sigma'_{zz} = \dot{\varepsilon}_{xx} + \dot{\varepsilon}_{yy} + \dot{\varepsilon}_{zz} = 0$ for incompressive ice. For linear extension, $\dot{\varepsilon}_{yy} = 0$ and $\sigma_T = 2\sigma'_{xx}$. For radial extension, $\dot{\varepsilon}_{xx} = \dot{\varepsilon}_{yy}$ and $\sigma_T = 3\sigma'_{xx}$. For pure shear, $\dot{\varepsilon}_{xx} = -\dot{\varepsilon}_{yy}$ and $\sigma_T = \sigma'_{xx}$. Flow bands that widen and narrow along their lengths permit these and other combinations of $\dot{\varepsilon}_{xx}$ and $\dot{\varepsilon}_{yy}$. Flow bands lie in directions of maximum surface slope. They diverge from interior ice domes, converge on ice streams, and can both diverge and converge within ice shelves. Convergence and divergence are minimal in ice streams, so flow band width can be taken as constant to a first approximation in which $\dot{\varepsilon}_{yy} = 0$.

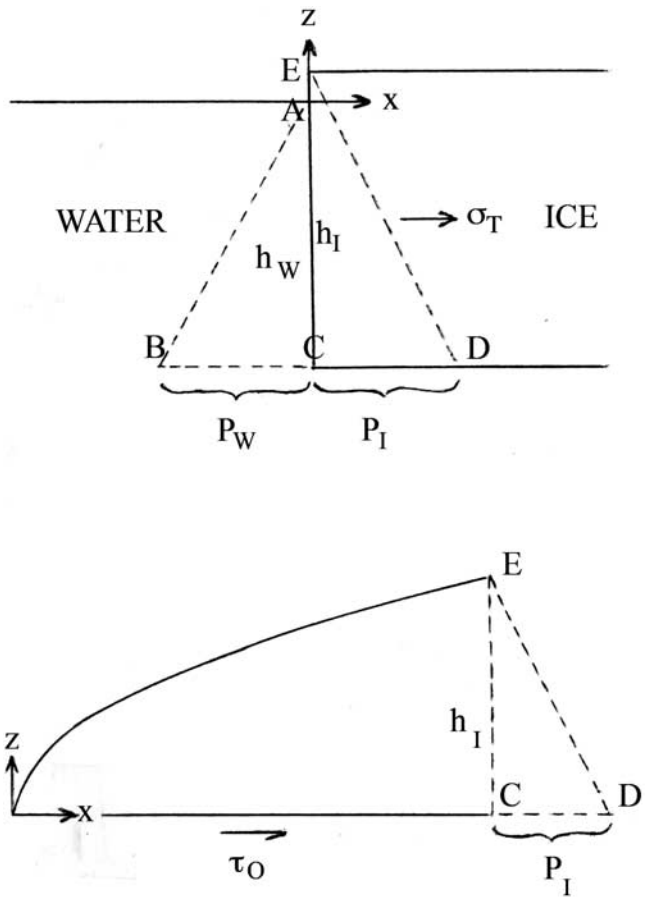

Figure 2. The horizontal force balance (top) for the calving front of an ice shelf and (bottom) for an ice sheet on a horizontal bed. Water and ice pressures increase linearly to P_W and P_I, respectively, at the base where $P_W = P_I$ in the ice shelf. For unit width of the ice shelf, net longitudinal driving force due to gravity is area *CDE* for ice minus area *ABC* for water and is resisted by longitudinal tensile force $\sigma_T h_I$ with tensile stress σ_T. For unit width of the ice sheet, the longitudinal driving force in ice is area *CDE* and is resisted by longitudinal shear force $\tau_O x$ with basal shear stress τ_O.

[11] *Weertman* [1957a] obtained σ_T for linear and radial shelf flow by integrating the equilibrium equations. *Robin* [1958] obtained the linear solution by balancing longitudinal forces at the calving front of an ice shelf, where ice thickness h_I is supported by water depth h_W. As seen in Figure 2 (top), his geometrical representation of longitudinal forces per unit flow band width w_I balances the net longitudinal force driving gravitational spreading $(F_G)_x = \bar{P}_I h_I w_I - \bar{P}_W h_W w_I$ against the force resisting gravitational spreading $(F_R)_x = \sigma_T h_I w_I$ for linear flow, where $\bar{P}_I = \frac{1}{2}P_I$ and $\bar{P}_W = \frac{1}{2}P_W$, with $P_I = P_W$ at the base so that $\rho_I h_I = \rho_W h_W$ in equations (2) and (3). Then $\bar{P}_I h_I$ is triangular area *CDE* for ice and $\bar{P}_W h_W$ is triangular area ABC for water. Setting $(F_G)_x = (F_R)_x$ and $\sigma_W h_I = \bar{P}_W h_W$ for compressive stress σ_W from water buttressing, σ_T is:

$$\sigma_T = \bar{P}_I - \sigma_W = \bar{P}_I - \bar{P}_W(h_W/h_I) = \bar{P}_I(1 - h_W/h_I) = \frac{1}{2}\rho_I g h_I(1 - \rho_I/\rho_W) = \bar{P}_I(h/h_I) \quad (5)$$

Here $\sigma_W = \bar{P}_W(h_W/h_I)$ opposes $\bar{P}_I = \frac{1}{2}\rho_I g h_I$, and $h = h_I - h_W = h_I(1 - \rho_I/\rho_W)$ is ice height above water. Figure 2 (bottom) is the geometrical representation of the longitudinal force balance applied by *Nye* [1951] to an ice sheet on a horizontal bed where basal shear stress τ_O is constant. The longitudinal force causing gravitational spreading is $(F_G)_x = \bar{P}_I h_I w_I = \frac{1}{2}\rho_I g h_I^2 w_I$ with longitudinal gravitational motion at distance x from the ice margin resisted by τ_O acting on basal area $w_I x$, giving resisting force $(F_R)_x = \tau_O w_I x$. Setting $(F_G)_x = (F_R)_x$ and solving for x:

$$x = \bar{P}_I h_I/\tau_O = (\rho_I g/2\tau_O)h_I^2 \quad (6)$$

where $\bar{P}_I h_I$ is the area of gravitational triangle CDE. Equation (6) gives a parabolic ice sheet surface profile. Differentiating and solving for τ_O, taking $\alpha = dh_I/dx$ as the ice surface slope, gives the shallow ice approximation of the equilibrium equations:

$$\tau_O = \rho_I g h_I \alpha = P_I \alpha \quad (7)$$

For the same P_I in a flow band, $\sigma_T \gg \tau_O$ because $h/h_I \gg 2\alpha$.

[12] The concave surface of streamflow connects the high convex surface of sheet flow to the low flat surface of shelf flow in Figure 2. Since sheet flow is fully grounded and shelf flow is fully floating, streamflow must result from a progressive downstream transition from fully grounded to fully floating conditions. By analogy with equations (2) and (3), define a "floating fraction" φ of ice along the ice streams as follows:

$$\phi = \frac{w_F}{w_I} = \frac{h_F^*}{h_I} = \frac{h_W^*(\rho_W/\rho_I)}{h_I} = \frac{\rho_W h_W^*}{\rho_I h_I} = \frac{P_W^*}{P_I} \quad (8)$$

where "effective" basal water pressure P^*_W "floats" ice over width w_F of total flow band width w_I and $h^*_F = h^*_W(\rho_W/\rho_I)$ is an "effective" height of ice that floats in water of "effective" height h^*_W above the bed, as shown in Figure 3. Then h^*_F/h_I become an effective proxy for real floating fraction $\varphi = w_F/w_I$ of ice in ice of height h_I. In Figure 3, take $h^*_F \equiv h_F$ and $h^*_W \equiv h_W$. Then by definition from equation (8):

$$h_F = h_W(\rho_W/\rho_I) = h_I\phi = h_I(w_F/w_I) \quad (9)$$

In equation (8), $P^*_W = \rho_W g h^*_W$ is different from $P_W = \rho_W g h_W$ in equation (2) because P^*_W is a mathematical quantity whereas P_W is a real physical quantity. In the horizontal force balance, longitudinal deviator stresses resist longitudinal gravitational motion. An effective P^*_W is needed to relate floating width w_F to the geometrical representation of gravitational driving forces linked to the floating component of streamflow across width w_I. This linkage then relates φ to the resisting stresses.

[13] Equations (2) and (3) come from the vertical force balance in which $P_W \approx P_I$ for both floating ice and ice grounded on a wet bed. In floating width w_F and in grounded width $w_I - w_F$ of the flow band, P_W can be slightly different from and usually less than P_I due to gradients in basal water pressure that allow some basal

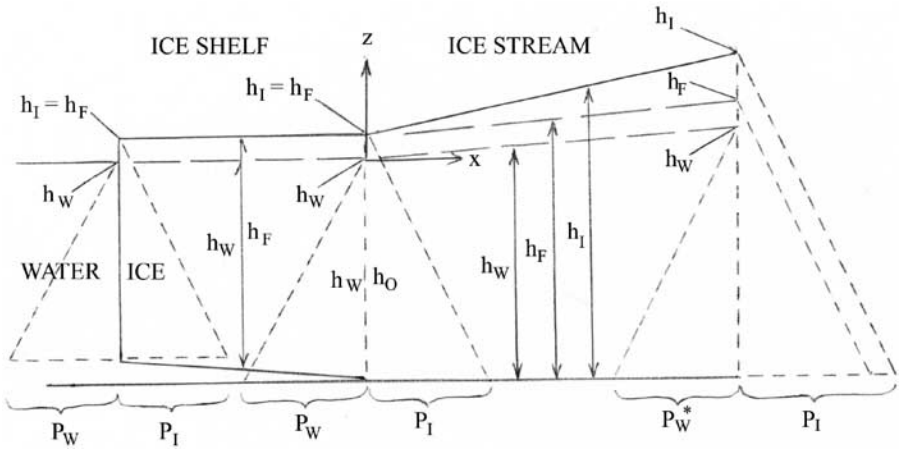

Figure 3. The gravitational component of the horizontal force balance for shelf flow and streamflow at three locations. The difference in areas of the dashed triangles at the ice shelf calving front (left), the ice shelf ice stream grounding line (middle), and up the ice stream (right) is $1/2P_I h_I - 1/2P_W h_W$ for floating ice (left and middle) and $1/2P_I h_I - 1/2P^*_W h_W$ for partly grounded ice (right), where P^*_W is an "effective" basal water pressure that represents the floating fraction of ice. The difference in area of triangles at each location is the net longitudinal driving force due to gravity per unit flow band width w_I. For partly floating ice in the ice stream, h_W is an effective water height that gives effective water pressure P^*_W in basal ice, $h_F = (\rho_W/\rho_I)h_W$ is an effective ice height that floats in water height h_W, and h_I is ice height above the ice base, where $\phi = h_F/h_I = P^*_W/P_I$ is the floating fraction of the ice such that $\varphi = 1$ for the ice shelf and $1 > \varphi > 0$ for the ice stream, with $h_I = h_O$ at the grounding line ($x = 0$). When basal water is produced faster than it leaks away downstream, $h_F > h_O$ as shown and the ice stream lengthens. If leakage exceeds production, $h_F < h_O$ and the ice stream shortens. An ice ridge forms when h_F decreases sharply for $x > 0$. Appendix A shows how partitioning the net gravitational driving force delivers stresses σ_T, τ_O, and τ_S that resist gravitational motion in stream flow.

water to "leak away" downstream [see *Engelhardt and Kamb*, 1997; *Kamb*, 2001]. Equations (8) and (9) come from the horizontal force balance for which $0 < P^*_W < P_I$ along directions of ice flow. For ice grounded on a rugged wet bed, horizontal ice flow is inhibited by bedrock bumps that penetrate basal ice [*Weertman*, 1957b]. Ice motion adds to basal ice pressure as ice pushes against bumps and may subtract from basal ice pressure as ice pulls away from bumps, so the net effect of P_W is zero. Equations (8) and (9) reflect this fact, whereas equations (1) and (2) do not. Here I borrow from an explanation provided by J. Weertman (personal communication, 2008):

> The term P^*_W defined by equation (8) is not a physical quantity. In general it is numerically smaller than the actual water pressure P_W under floating width w_F, which Kamb (2001) found was $P_W \approx 0.9\ P_I$ in dozens of boreholes through West Antarctic ice streams. Here P^*_W is a mathematical quantity, a pseudo water pressure, that can be represented geometrically in the horizontal force balance.

[14] In equation (8), suppose that all portions of flow band width w_I for which bedrock bumps are drowned add up such that $w_F = 0.7\ w_I$, so that $\varphi = 0.7$ is the floating fraction of ice. Horizontal ice motion is retarded where ice is grounded on portions that add up to $w_I - w_F = 0.3\ w_I$. The height of ice is h_I for both floating and grounded portions, but the fraction of h_I that represents ice bed uncoupling is effective flotation height $h_F = h_I(w_F/w_I) = \varphi\ h_I = 0.7\ h_I$ given by equation (9). Basal resistance to horizontal ice motion is provided only by effective height $h_I - h_F = 0.3\ h_I$ above effective flotation height h_F. This part of the ice overburden is "pinned" to the bed at bedrock bumps that retard horizontal ice flow. Similarly, spreading of a floating ice shelf is retarded by basal pinning points identified by ice rises and ice rumples on the surface. Floating fraction φ of ice quantifies ice bed uncoupling that converts sheet flow to shelf flow by way of stream flow.

[15] In Figure 3, longitudinal tensile stress σ_T acting on ice thickness h_I per unit flow band width w_I balances the difference in area between the opposing driving force triangles, $\frac{1}{2}P_I h_I - \frac{1}{2}P_W h_W$, due to gravity in ice and water. In shelf flow, $\frac{1}{2}P_W h_W$ is the actual physical force water exerts against ice in the horizontal x direction, but this physical contact is missing in stream flow. Yet the effect of $\frac{1}{2}P_W h_W$ cannot just vanish for $x > 0$ upstream from the ice shelf grounding line because then streamflow would not be a transition from sheet flow to shelf flow. Although horizontal back force $\frac{1}{2}P_W h_W$ due to direct contact over water height h_W vanishes when $x > 0$, a water-related back force must exist upstream. This requirement is met by postulating for $x > 0$ a longitudinal force balance for water, $\frac{1}{2}P^*_W h_W = \sigma_W h_I$, where $\sigma_W = \frac{1}{2}P^*_W(h_W/h_I)$ is a compressive back stress acting across ice thickness h_I that would be produced by effective water height h_W.

[16] In addition, as seen in Figure 3, ice partially grounds when $x > 0$, so area $\frac{1}{2}P_I h_I - \frac{1}{2}P^*_W h_F$ is another horizontal back force per unit flow band width w_I that resists gravitational flow. This additional back force in ice streams is caused by ice bed contact that introduces basal and side drag. Basal and side drag produce basal and side shear stresses τ_O and τ_S, respectively, that act on ice all the way to the (un)grounding line. Side shear

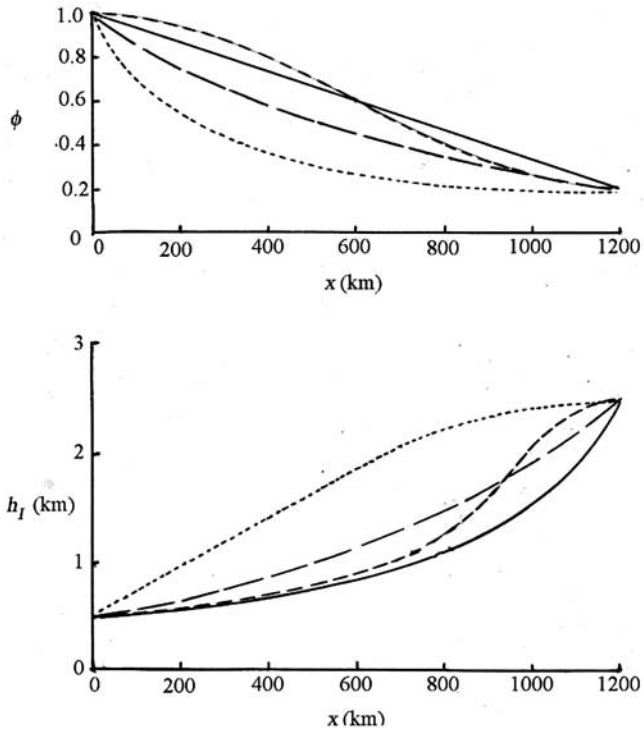

Figure 4. Ice stream profiles resulting from progressive downstream reductions of ice bed coupling. (top) Reductions in floating fraction φ along distance x for an ice stream with $\varphi = 1$ and $h_I = h_O = 500$ m at $x = 0$ and $\varphi = 0.2$ and $h_I = h_L \approx 2500$ m at $x = L = 1200$ km. (bottom) Ice elevations h_I above a horizontal bed for these reductions in φ. Solid lines are from equation (11). Long dashed curves are for $c_1 = 0$, $c_2 = 1$, and $\lambda = 1.61$ in equation (12). Dotted curves are for $c_1 = 0.2$, $c_2 = 0.8$, and $\lambda = 5$ in equation (12) and give the convex profile seen in ice ridges between ice streams. Short dashed curves are from equation (13). Smooth decreases of φ along x allow concave surfaces downstream that become convex upstream.

exists because ice ridges between ice streams are more fully grounded. Therefore, instead of using a net gravitational driving force, it is more appropriate to make $(F_G)_x = \frac{1}{2}P_I h_I$ the only driving force and to relate resisting forces to tensile and compressive longitudinal stresses σ_T and σ_W for floating fraction φ and to basal and side shear stresses τ_O and τ_S for grounded fraction $1 - \varphi$.

[17] The first fact in glaciology is ice height above the bed is determined by ice bed coupling that resists gravitational lowering and spreading of ice. First approximations for the height of an ice sheet above a horizontal bed were the parabolic profile for a constant basal shear stress τ_O [*Nye*, 1951], and elliptical profiles when a constant surface accumulation rate allowed τ_O to vary for a thawed bed [*Nye*, 1959] using the *Weertman* [1957b] sliding law and a frozen bed [*Haefeli*, 1961] using the *Glen* [1955] flow law. Thawing a frozen bed lowers the ice surface about 20% and freezing a thawed bed raises the ice surface about 25% [*Hughes*, 1981]. In both cases the ice surface remains convex and high because thawing a frozen bed weakens ice bed coupling but keeps ice in direct contact with the bed everywhere. Once the bed is fully thawed, however, additional water cannot spread out over the bed; it can only deepen. Deepening will be greatest in bedrock hollows, producing subglacial lakes [*Siegert et al.*, 1996; *Oswald and Gogineni*, 2008].

[18] Where deepening of basal water collects in bedrock channels aligned in directions of steepest ice surface slopes, ice bed uncoupling increases downslope because the pressure gradient of basal water drives water downslope. Basal water will "carry" the overlying ice in these downslope directions. Overlying ice will then move faster than flanking ice and slow sheet flow becomes fast streamflow in these channels. Along stream flow, the high convex surface of sheet flow driven by the product of ice thickness and surface slope, equation (7), becomes the low flat surface of shelf flow driven by ice height floating above water, equation (5). To accomplish this, streamflow must have a concave profile with $0 < \varphi < 1$ and φ increasing downslope to convert the high convex surface ($\varphi = 0$) into the low flat surface ($\varphi = 1$). The simplest expression accomplishing this is

$$\varphi = h_O/h_I \tag{10}$$

where $h_I = h_O$ at $x = 0$, with x positive against ice flow.

[19] In pure shelf flow, ice is fully floating (uncoupled) and ice thickness is constant everywhere, so $h_O = h_I$ all along x, giving $\varphi = 1$ in equation (10), with $\tau_O = 0$ and σ_T given by equation (5). In pure sheet flow, ice is fully grounded (coupled) and h_I increases along x from $h_O = 0$ at $x = 0$, giving $\varphi = 0$ in equation (10), with $\sigma_T = 0$ and τ_O given by equation (7). This produces a convex ice surface profile, such as the parabolic profile given by equation (6) for constant τ_O on a horizontal bed. In pure stream flow, a gradual decrease of φ along x for finite h_O at $x = 0$ in equation (10) gives gradual coupling and a concave ice surface profile, so long as φ remains finite. A rapid decrease of φ along x gives a convex profile for more rapid coupling, such as exists for ice ridges that lie between closely spaced ice streams.

[20] In applying equation (10) to ice streams, it is necessary that $h_O > 0$ at $x = 0$ and $\varphi_L > 0$ at $x = L$ for an ice stream of length L. Then h_I and φ remain finite. For a linear decrease of φ along x:

$$h_I = \frac{h_O}{\phi} = \frac{h_O}{1 - (1 - \phi_L)x/L} \tag{11}$$

For an exponential decrease of φ along x:

$$h_I = \frac{h_O}{\phi} = \frac{h_O}{c_1 + c_2 e^{-\lambda(x/L)}} \tag{12}$$

For a cosine-squared decrease of φ along x:

$$h_I = \frac{h_O}{\phi} = \frac{h_O}{\phi_L + (1 - \phi_L)\cos^2(\pi x/2L)} \tag{13}$$

[21] Equations (11) through (13) are plotted in Figure 4 for $h_O = 500$ m, $L = 1200$ km, and $\varphi_L = 0.2$. A linear decrease of φ along x from equation (11) delivers a concave ice stream profile. An exponential decrease of φ along x from equation (12) delivers a concave profile when $c_1 = 0$, $c_2 = 1$ and

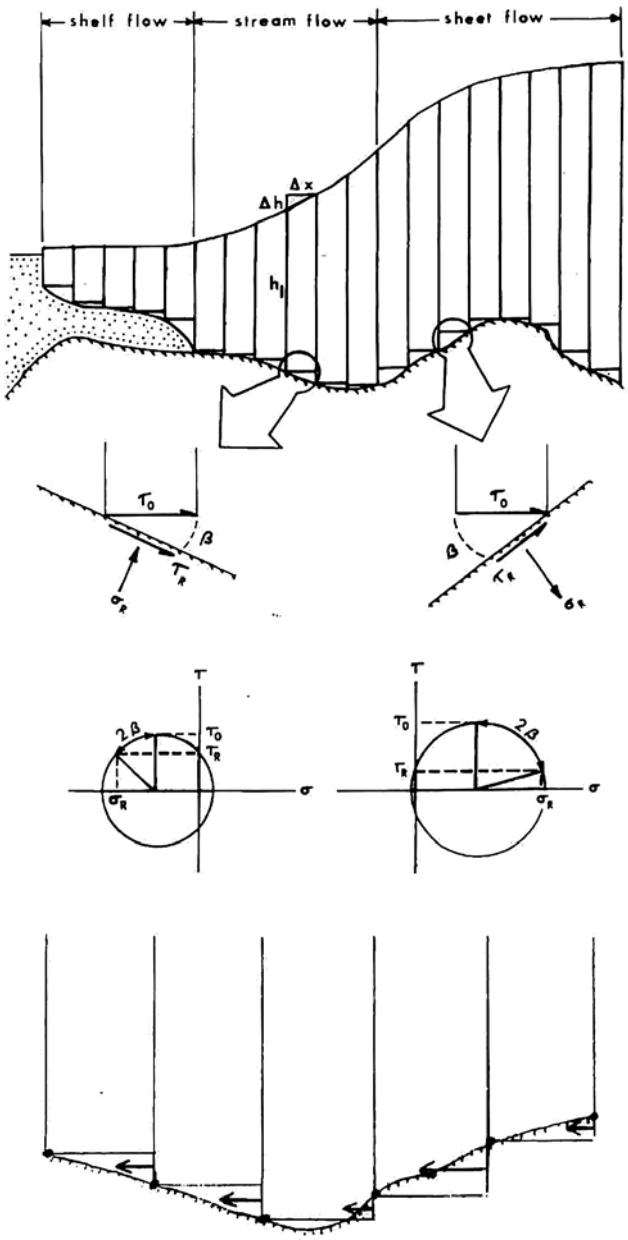

Figure 5. Representation of the bed beneath an ice sheet flow band as a sequence of upward or downward steps. Constant step lengths Δx have variable step heights Δh_B. Ice columns above each step have height h_I on the low side and surface slope $\Delta h/\Delta x$. (top) Basal shear stress τ_O at the base of each ice column can be resolved into two deviator components, a shear stress τ_R parallel to the bed and a normal stress σ_R perpendicular to the bed using Mohr circles. If the bed slopes upward in the direction of ice flow, σ_R is compressive. If the bed slopes downward in the direction of ice flow, σ_R is tensile. A compressive σ_R deposits lodgment till and a tensile σ_R quarries jointed bedrock. (bottom) When ice columns touch the bed in the flow direction, normal stress σ_N between steps (arrows) is tensile and quarries bedrock by basal freezing on down steps (right) but is compressive and deposits till by basal melting on up steps (left).

$\lambda = 1.61$, but a convex profile when $c_1 = 0.2$, $c_2 = 0.8$, and $\lambda = 5$, for example. A cosine–squared decrease of φ along x from equation (13) delivers a concave profile that becomes convex as x increases. These results show that how φ decreases along x allows a variety of concave ice stream profiles, and also produces the convex profiles of ice ridges between ice streams. A convex profile also results when φ decreases too slowly along x, such as beyond the head of ice streams.

[22] Equation (10) fails to deliver the profile of a marine ice sheet on a frozen bed, for which $h_O > 0$ and $\varphi = 0$, so that h_I is infinite. Therefore, equation (10) requires a thawed bed, a limitation that does not exist in equation (8), which defines φ. For a marine ice stream, $h_O = h_I$ at the grounding line of its floating ice tongue where $\varphi = 1$. For a terrestrial ice stream, $h_O \rightarrow h_I$ at the minimum slope of its grounded ice lobe where $\varphi \rightarrow 1$.

3. Deriving the Stresses in Ice Streams

[23] Bed topography along an ice sheet flow band is approximated by the up-down staircase shown in Figure 5, with steps of constant length Δx and variable heights $\pm\Delta h_B$ for bed height $+h_B$ or depth $-h_B$ with respect to sea level. Taking x horizontal and z vertical for flow band width w_I, basal longitudinal force F_N normal to areas $A_N = w_I\,\Delta h_B$ give normal stresses $\sigma_N = F_N/A_N$ that are tensile when ice pulls away from steps and compressive when ice pushes against steps. These stresses are ignored compared to gravitational driving stresses $\sigma_G = P_I\,\Delta h/\Delta x$ for basal ice pressure P_I and ice surface slope $\Delta h/\Delta x$ due to ice elevation change Δh in step Δx. This limitation is acceptable when bed slopes are comparable to or less than surface slopes [*Hughes*, 1998, pp. 144–145]. It allows forces to be balanced on successive vertical columns of ice, each with a horizontal base of area $A_O = w_I\,\Delta x$ where the basal shear stress is τ_O, as distinct from basal shear stress τ_R resolved along a sloping bed, as shown in Figure 5. A horizontal bed (see Figure 3) eliminates the staircase.

[24] In ice streams, effective flotation height $h_F = h_W(\rho_W/\rho_I) = h_I\phi = h_I(w_F/w_I)$ above the bed is less than ice height h_I above the bed, where h_F is a proxy for portion w_F of flow band width w_I within which ice is supported by actual basal water pressure $P_W \approx P_I$. Effective pressure P_W^* occurs across w_I, according to equation (8). The relationship of h_F to h_I and h_W is shown by the gravitational force triangles in Figures 3 and 6. Upstream from the ice shelf grounding line, the horizontal gravitational driving force in ice per unit flow band width given by area $\bar{P}_I h_I$ of the big triangle includes the shaded area in addition to water triangle 1 and ice triangle 2 respectively linked to σ_W and σ_T for shelf flow. Here σ_W is the compressive stress of water on ice such that $\sigma_W h_I = \bar{P}_W h_W$ from the calving front to the grounding line and $\sigma_W h_I = P_W^* h_W$ in from the grounding line. This shaded area in Figure 6 represents the additional gravitational force needed to overcome the added resistance to ice flow caused by partial grounding. Partial grounding under the ice stream adds basal shear stress τ_O. Additional grounding across the sides of the ice stream adds side shear stress τ_S. These shaded areas in successive gravitational force triangles upstream from the grounding line are the geometrical representations of gravitational forcing needed to overcome basal and side shear.

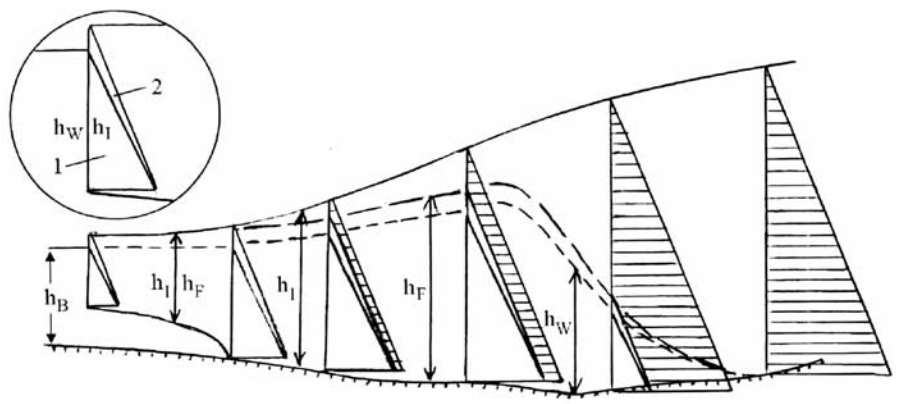

Figure 6. A geometrical representation of gravitational forces along an ice sheet flow band. Sheet flow (right) becomes streamflow (middle) that ends in shelf flow (left). The triangles represent the downslope gravity force, with triangle bases being the pressure of basal ice or water and triangle heights being ice thickness h_I to the ice surface, flotation ice thickness h_F to the long dashed line, and water thickness h_W to the short dashed line that floats ice thickness h_F. Shaded parts of the triangles are balanced by basal and side shear forces. Unshaded parts of the triangles are balanced by a compressive force pushing on h_W in water triangle 1 and a tensile force pulling on h_I in ice triangle 2. The circled inset identifies triangles 1 and 2 at the calving front. These triangles exist as long as $h_W > 0$. For partly floating ice in stream flow, h_F and h_W are "effective" heights of ice and water linked to "effective" basal water pressure P_W^* as a mathematical quantity that permits the geometrical representation of gravitational forces driving longitudinal ice flow.

[25] In the shaded areas of the gravitational force triangles in Figure 6, the triangle above h_F is linked to basal shear stress τ_O, and the parallelogram below h_F is linked to side shear stress τ_S. Note that the triangular shaded area grows as h_F decreases upstream, until this area coincides with $\bar{P}_I h_I$ when $h_F = 0$. This is the condition for pure sheet flow, in which only τ_O resists gravitational forcing. Also note that the size ratio of the shaded triangle to the shaded parallelogram changes as h_F changes, with the ratio increasing upslope toward the ice divide and decreasing downslope toward the (un)grounding line. Therefore, basal shear replaces side shear upslope and side shear replaces basal shear downslope, even though both basal and side shear vanish at the (un)grounding line. There is no side shear after the ice stream becomes fully afloat, so the geometrical force balance is limited to ice stream flow bands that continue as ice shelf flow bands and move with essentially the same speed as the ice shelf. Buttressing of ice streams by an ice shelf is due to basal pinning points and side shear in a confining embayment. Side shear in individual ice stream flow bands vanishes when the flow bands become imbedded in the ice shelf. When applied to ice streams that end as ice lobes grounded on land, $\tau_S = 0$ along the sides of an ice lobe, but τ_O increases toward the lobe terminus as basal water escapes, thereby giving the ice lobe a low convex profile (see *Hughes* [2003, Figure 7e]; however, P_W^*/P_I should approach zero, not unity, toward the lobe margin).

[26] Downslope resistance to ice flow contributes to the size of triangular area $\bar{P}_I h_I$ that represents the horizontal gravitational driving force in ice per unit flow band width. For stream flow, this means that at any point along an ice–stream flow band having transverse cross-sectional area $A_x = h_I w_I$, a longitudinal force balance equates longitudinal gravitational driving force $\bar{P}_I A_x$ with all the downstream resistance to flow, which is represented locally by compressive force $\sigma_C A_x$ that "pushes" downstream ice, and any remaining local tensile force $\sigma_T A_x$ that "pulls" upstream ice. Dividing by A_x gives

$$\bar{P}_I = \sigma_C + \sigma_T \tag{14}$$

where σ_C and σ_T are the respective compressive and tensile stresses. Equation (14) was first applied to ice streams buttressed by ice shelves in a force perturbation study by *Thomas* [2004]. A small local perturbation in σ_C caused by small far-field downstream reductions in resistance to flow, including a small reduction in ice shelf buttressing, causes a big local perturbation in σ_T because $\sigma_C \gg \sigma_T$ and $\bar{P}_I$ has no immediate change. Note the similarity between equation (14) for streamflow in which $\bar{P}_I > \bar{P}_W^*$ and equation (5) for shelf flow in which $\bar{P}_I = \bar{P}_W$. They are identical except that σ_C replaces σ_W, where $\sigma_W = \bar{P}_W(h_W/h_I)$ is the compressive back stress in ice caused by water "dammed" by ice at the grounding line. Therefore, σ_C can be understood if $\bar{P}_W^*$ is partly a result of local "damming" of basal water that cannot "leak away" by flowing downstream. This reduces access of basal water to the sea because downstream ice thinning by extending flow has been reduced by basal and side shear, grounding line water pressure, and ice shelf buttressing. All these thicken ice because increased gravitational forcing is needed to balance the increased downstream resistance to ice flow. The proxy for downslope resistance is local force $\sigma_C A_x$ that vanishes when downslope resistance vanishes, leaving $\bar{P}_I = \sigma_T$ in equation (14), where σ_T is a tensile stress that "pulls" upslope ice, see the "thought experiment" of *Hughes* [2003].

[27] Taken together, all four stresses σ_C, σ_T, τ_O, and τ_S can be expressed in terms of floating fraction φ of ice at any location along an ice stream flow band. This is done with the assistance of Figure 7 (top). The shaded area above

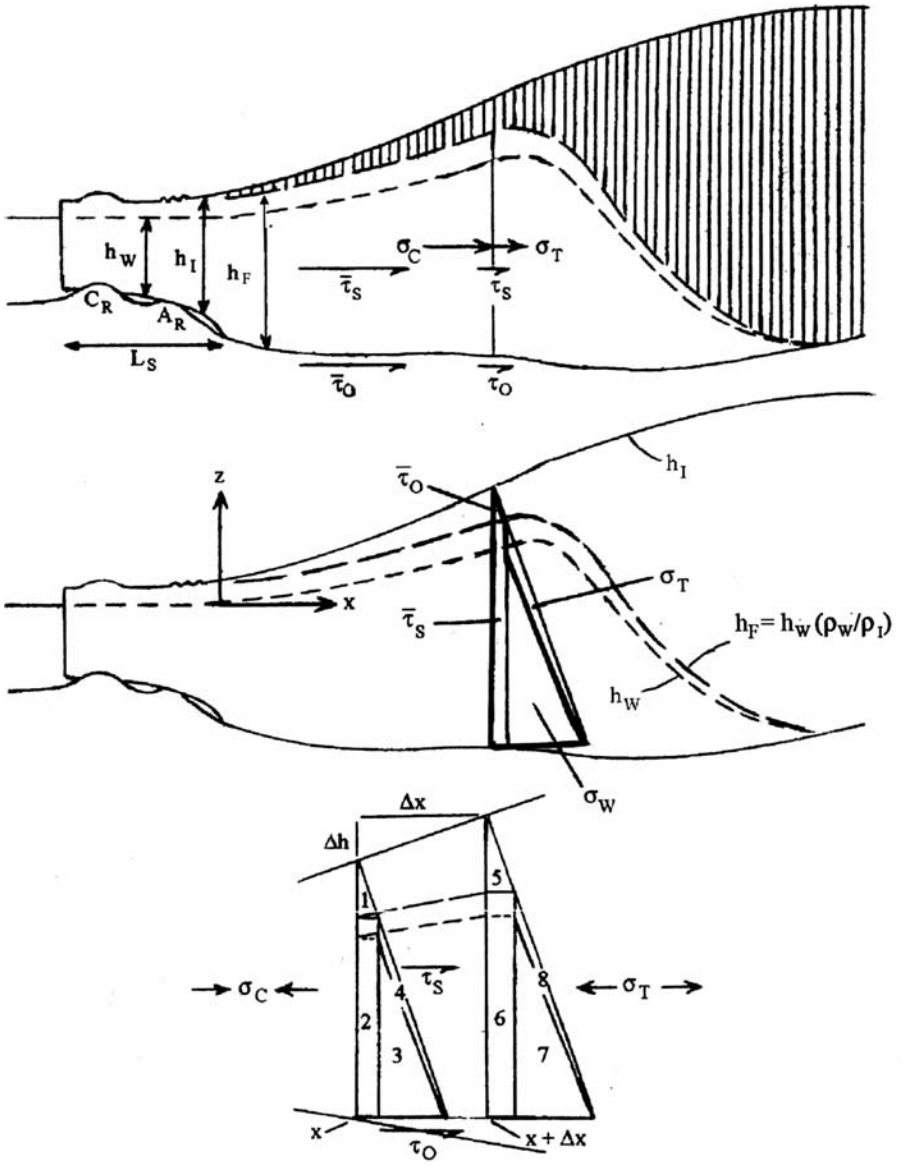

Figure 7. The longitudinal geometrical force balance on an ice stream ending as a confined ice shelf. (top) Longitudinal stresses that resist gravitational flow. The bed supports ice in the shaded area. Ice in the unshaded area is supported by basal water pressure. (middle) Gravitational forces at x represented as triangles and a rectangle are linked to specific resisting stresses. The area inside the thick border is linked to σ_C. Heights h_I, h_W, and h_F are measured from the bed for $x > 0$. (bottom) Resisting stresses and gravitational forces along Δx. Resisting and gravitational forces are balanced between x and $x + \Delta x$. Actual basal water pressure P_W in fully floating shelf flow becomes effective basal water pressure P_W^* in partly grounded stream flow.

$h_F = h_W(\rho_W/\rho_I) = h_I\phi$ is the portion of the ice overburden that has direct contact with basal rock or till across flow band width w_I when treating drag resistance to downstream ice flow. The unshaded area below h_F has no contact with the bed and must be supported by basal water pressure when treating stretching resistance to flow. Applying equation (8), $\phi = w_F/w_I = P_W^*/P_I$ averaged across flow band width w_I determines h_W.

[28] Further quantification is obtained by taking axis x horizontal and positive against flow, with $x = 0$ at the ice shelf grounding line, and taking axis z vertical and positive upward, with $z = 0$ at sea level. At positive x, stresses σ_T, τ_O, and τ_S are respectively local longitudinal tensile, basal shear, and side shear stresses, whereas longitudinal compressive stress σ_C acts as a local proxy for downslope resistance to ice flow caused by basal and side shear all the way to the ice shelf calving front, and to mean water pressure $(\bar{P}_W)_O$ at the grounding line. *Thomas* [2004] did the same, but without φ in these stresses. Shear resistance in ice shelves includes basal shear over pinning points of area A_R that produce ice rumples on the surface, side shear around pinning points of circumference C_R that produce ice rises on the surface, and side shear along grounded length L_G of an ice shelf in a confining embayment, with $L_G = 2L_S$ for grounded parallel sides of length L_S. More generally, L_S is related to the longitudinal component of L_G on each side.

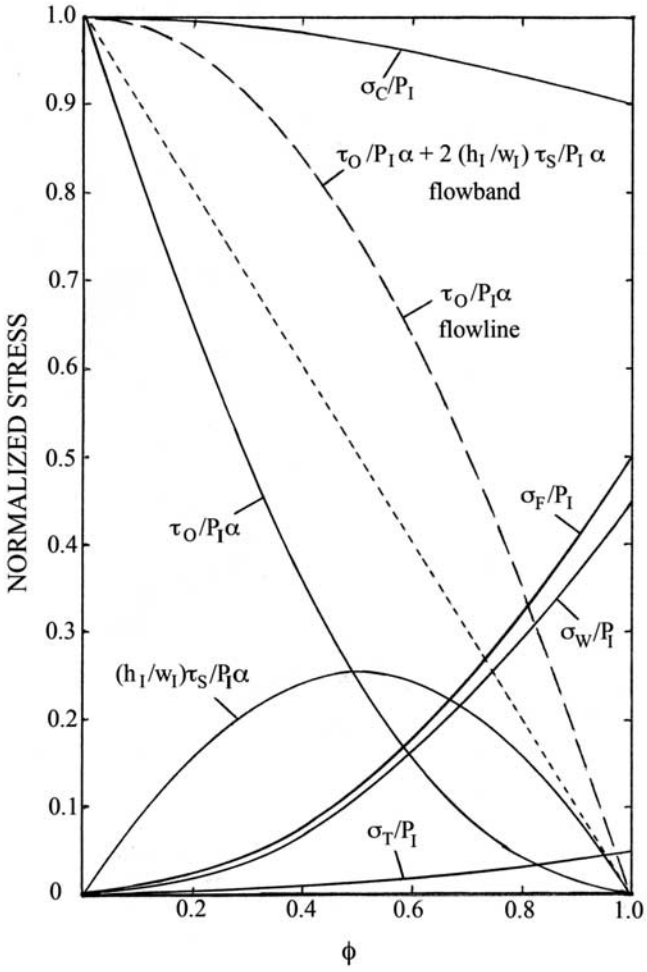

Figure 8. Variations of normalized stresses in Table 1 with floating fraction φ of ice. Solid curves are for flow bands. Long dashed curve $\tau_O/P_I\,\alpha$ for a flow line is identical to $\tau_O/P_I\alpha + 2(h_I/h_W)\,\tau_S/P_I\alpha$ for a flow band. The linear short dashed line is a plot of $\tau_O/P_I\alpha + (h_I/h_W)\,\tau_S/P_I\alpha$ for flow bands.

Shear over and around basal pinning points generates compressive flow on the stoss side. This contributes to σ_C farther upstream at x. Downstream shear stresses are represented by average basal shear stress $\bar{\tau}_O$ and average side shear stress $\bar{\tau}_S$ in Figure 7 (top). These stresses vary locally.

[29] A geometrical representation of gravitational stresses at x on the ice stream flow band is shown in Figure 7 (middle). The large triangle having area $\bar{P}_I h_I$ represents the gravitational force in ice per unit flow band width w_I. In relating it to equation (14), σ_C is linked to the area enclosed by the heavy black border, within which is a water triangle below h_W linked to σ_W, an ice triangle above h_F linked to $\bar{\tau}_O$, and an ice rectangle below h_F linked to $\bar{\tau}_S$, leaving an ice triangle below h_F that must be linked to σ_T. This is ice triangle 2 all along x in Figure 6. Then $\sigma_T \ll \sigma_C < \bar{P}_I$, as in the force perturbation analysis by *Thomas* [2004]. The shaded triangle and parallelogram in Figure 6 have the same respective areas as the triangle linked to $\bar{\tau}_O$ and the rectangle linked to $\bar{\tau}_S$ in Figure 7 (middle). Appendix A shows how all stresses are geometrically linked to φ.

[30] By analogy with linear shelf flow, but with $\bar{P}^*{}_W = \bar{P}_I\phi$ and $h_F = h_W(\rho_W/\rho_I) = h_I\phi$ according to equation (8), derivations in Appendix A show that

$$\sigma_F = \bar{P}^*_W(h_F/h_I) = (\bar{P}_I\phi)\phi = \bar{P}_I\phi^2 \tag{15}$$

$$\sigma_W = \bar{P}^*_W(h_W/h_I) = (\bar{P}_I\phi)(\rho_I/\rho_W)\phi = \bar{P}_I(\rho_I/\rho_W)\phi^2 \tag{16}$$

$$\sigma_T = \sigma_F - \sigma_W = \bar{P}_I(1-\rho_I/\rho_W)\phi^2 \tag{17}$$

$$\sigma_C = \bar{P}_I - \sigma_T = \bar{P}_I - \bar{P}_I(1-\rho_I/\rho_W)\phi^2 = \bar{P}_I\left(1-\phi^2\right) + \sigma_W \tag{18}$$

Note that $\sigma_C = \sigma_W$ when $\varphi = 1$ for shelf flow.

[31] As in the work by *Thomas* [2004], compressive stress σ_C at x results from all downstream resistance to ice flow. A longitudinal force balance for constant w_I gives, referring to Figure 7 (top):

$$\sigma_C A_x = \sigma_C h_I w_I = \bar{\tau}_O(w_I x + A_R) + \bar{\tau}_S \cdot \left(2\bar{h}_I x + 2\bar{h}_S L_S + \bar{h}_R C_R\right) + (\bar{P}_W h_W)_O w_I \tag{19}$$

where $\bar{\tau}_O$ is the average basal shear stress over downslope basal area $w_I\,x$ of the ice stream and basal area A_R of ice rumples on the ice shelf, $\bar{\tau}_S$ is the average side shear stress over downslope side areas $2\bar{h}_I\,x$ of the ice stream, $2\bar{h}_S L_S$ of the ice shelf, and $\bar{h}_R C_R$ of ice rises on the ice shelf for average ice thickness $\bar{h}_I$ along length x of the ice stream, $\bar{h}_S$ along grounded side lengths L_S of the ice shelf, and $\bar{h}_R$ around circumference C_R of ice rises, and $(\bar{P}_W h_W)_O\,w_I$ is the back force at $x = 0$ due to average water pressure $\bar{P}_W$ in water of depth h_W at the ice shelf grounding line. In equation (19), therefore, compressive force $\sigma_C\,A_x$ at x on the left side is the result of average downslope basal and side shear forces and a water pressure force at $x = 0$, all on the right side. Solving for σ_C,

$$\sigma_C = \frac{\bar{\tau}_O(w_I x + A_R) + \bar{\tau}_S\left(2\bar{h}_I x + 2\bar{h}_S L_S + \bar{h}_R C_R\right) + (\bar{P}_W h_W)_O w_I}{h_I w_I} \tag{20}$$

Downslope driving force $(F_G)_1$ due to gravity at x is w_I times the area of triangle 1 in Figure 7 (bottom). It is resisted by a downslope basal shear force $(F_O)_1$ given by mean downslope basal shear stress $\bar{\tau}_O$ times basal area $w_I\,x$ beneath the ice stream and total area A_R beneath ice rumples on the ice shelf. Since triangle 1 occupies the shaded area in Figure 7 (top), its basal ice pressure $(P_I)_1 = \rho_I\,g(h_I - h_F)$ is supported by the bed and its mean downstream ice pressure $(\bar{P}_I)_1 = \frac{1}{2}(P_I)_1$ is exerted over area w_I times triangle height $h_I - h_F$. Equating this negative downslope driving force due to gravity $(F_G)_1 = -\frac{1}{2}(P_I)_1\,(h_I - h_F)w_I = -\frac{1}{2}\rho_I\,g(h_I - h_F)^2\,w_I$ and positive downslope resisting force $(F_O)_1 = \bar{\tau}_O(w_I\,x + A_R)$ to zero and solving for $\bar{\tau}_O$ using $h_F = h_I\phi$ gives

$$\bar{\tau}_O = \frac{(1/2)\rho_I g(h_I - h_F)^2 w_I}{w_I x + A_R} = \frac{(1/2)\rho_I g h_I(1-\phi)^2 h_I w_I}{w_I x + A_R} = \frac{\bar{P}_I(1-\phi)^2 h_I w_I}{w_I x + A_R} \tag{21}$$

Triangular areas 1, 3, and 4 in Figure 7 (bottom) have now been linked to $\bar{P}_I$ and φ through stresses $\bar{\tau}_O$, σ_W, and σ_T, respectively. All that remains is the area of rectangle 2 in Figure 7 (bottom) and $\bar{\tau}_S$ for side shear averaged over downslope side areas $2\bar{h}_I x$ of the ice stream and side areas $2\bar{h}_S L_S$ and $\bar{h}_R C_R$ of the ice shelf and ice rises having total grounded side lengths $2L_S$ and circumference C_R, respectively, as shown in Figure 7 (top). The negative downstream driving force due to gravity is given by w_I times the area of rectangle 2 for $(P_I)_1 = (P_I)_2$ and is $(F_G)_2 = -(P_I)_2$ $h_F w_I = -\rho_I g(h_I - h_F)h_F w_I$. It is resisted by positive downslope side shear force $(F_S)_2 = \bar{\tau}_S\,(2\bar{h}_I\, x + 2\bar{h}_S L_S + \bar{h}_R C_R)$. Summing these forces to zero and solving for τ_S using $h_F = h_I\phi$ gives:

$$\begin{aligned}\bar{\tau}_S &= \frac{\rho_I g(h_I - h_F)h_F w_I}{2\bar{h}_I x + 2\bar{h}_S L_S + \bar{h}_R C_R} = \frac{\rho_I g h_I(1-\phi)\phi h_I w_I}{2\bar{h}_I x + 2\bar{h}_S L_S + \bar{h}_R C_R} \\ &= \frac{P_I(1-\phi)\phi h_I w_I}{2\bar{h}_I x + 2\bar{h}_S L_S + \bar{h}_R C_R}\end{aligned} \tag{22}$$

Equation (14) can now be solved for φ using equations (17) and (18) for σ_T and σ_C, respectively. First, substitute equations (21) and (22) for $\bar{\tau}_O$ and $\bar{\tau}_S$ in equation (20):

$$\begin{aligned}\sigma_C &= \frac{(\bar{P}_W h_W)_O}{h_I} + \left[\frac{\bar{P}_I(1-\phi)^2}{w_I x + A_R}\right](w_I x + A_R) \\ &\quad + \left[\frac{P_I(1-\phi)\phi}{2\bar{h}_I x + 2\bar{h}_S L_S + \bar{h}_R C_R}\right]\left(2\bar{h}_I x + 2\bar{h}_S L_S + \bar{h}_R C_R\right) \\ &= \frac{1}{2}\rho_I g\left(h_O^2/h_I\right)(\rho_I/\rho_W) + \frac{1}{2}\rho_I g h_I(1-\phi)^2 + \rho_I g h_I(1-\phi)\phi \\ &= \frac{1}{2}\rho_I g h_O(\rho_I/\rho_W)(h_O/h_I) + \frac{1}{2}\rho_I g h_I\left(1 - 2\phi + \phi^2 + 2\phi - 2\phi^2\right) \\ &= \frac{1}{2}\rho_I g h_O(\rho_I/\rho_W)(h_O/h_I) + \frac{1}{2}\rho_I g h_I\left(1 - \phi^2\right)\end{aligned} \tag{23}$$

where equation (8) for $\varphi = 1$ at x = 0 gives $\bar{P}_W = \bar{P}_I$ and $h_W = h_O(\rho_I/\rho_W)$ for $h_I = h_O$. Combining equations (16) and (18) with equation (23) for σ_C and solving for φ gives:

$$\varphi = h_O/h_I \tag{24}$$

Equation (24) confirms equation (10). To a first-order approximation, it quantifies how marine ice sheets undergo rapid gravitational collapse. Collapse occurs up ice streams as ''salients'' of rapid surface lowering that extend the ice streams into the ice sheet. In this way the high convex surface of sheet flow collapses into the low flat surface of shelf flow. Calving bays can then migrate up the floating salients and carve out the heart of the ice sheet. Without equation (10), or something like it, the ice sheet would remain intact.

[32] A general decrease in floating fraction φ of basal ice toward the ice divide of an ice sheet is accomplished by increasing σ_C along x in equation (14), as seen in equations (18) and (23). Incremental increases in σ_C in incremental distance Δx results from adding incrementally to basal and side drag, respectively linked to τ_O and τ_S, so that tensile stress σ_T is reduced incrementally. Bed slopes are represented by an up–down staircase having constant step lengths Δx and variable step heights $\pm\Delta h_B$. Then the ice column in Figure 7 (bottom) has a horizontal base and basal shear stress τ_O, and column height changes by $\Delta h_I = \Delta h$ within each Δx step, taking Δh_B between steps. Tensile and compressive forces normal to step areas $w_I\Delta h_B$ are ignored because surface slopes are more important than bed slopes in the longitudinal force balance [see *Hughes*, 1998, pp. 144–145]. Figure 7 (bottom) shows stresses τ_O, τ_S, σ_T, and σ_C over length Δx in relation to changes in area of the triangles and rectangle from those shown as 1 through 4 at x to those shown as 5 through 8 at $x + \Delta x$ as flotation height h_F changes to $h_F + \Delta h_F$, where Δh_F can be an increase as shown or a decrease in h_F over Δx. For φ to decrease along x, Δh_F must decrease or an increase in Δh_F must be less than increase Δh in ice surface elevation.

[33] A longitudinal force balance that sums to zero negative driving force $(F_G)_x$ due to gravity as flow band width w_I times the difference between triangular areas 5 and 1 in Figure 7 (bottom) plus positive basal shear force $(F_O)_x = \tau_O\, w_I\, \Delta x$ gives for $\Delta x \to 0$

$$\begin{aligned}\tau_O &= \rho_I g h_I(1-\phi)\alpha - \rho_I g h_I(1-\phi)(\rho_W/\rho_I)\alpha_W \\ &= P_I[1-\phi][\alpha - (\rho_W/\rho_I)\alpha_W]\end{aligned} \tag{25}$$

where $\Delta h/\Delta x \to \alpha$ and $\Delta h_W/\Delta x \to \alpha_W$ as $\Delta x \to 0$. Equation (25) is derived in Appendix A.

[34] A longitudinal force balance that sums to zero negative driving force $(F_G)_x$ due to gravity as flow band width w_I times the difference between rectangular areas 6 and 2 in Figure 7 (bottom) plus positive side shear force $(F_S)_x = 2\tau_S\bar{h}_I\Delta x$ for $\bar{h}_I = h_I + \frac{1}{2}\Delta h_I$ gives for τ_S as $\Delta x \to 0$

$$\begin{aligned}\tau_S &= \frac{1}{2}\rho_I g w_I\phi\alpha + \frac{1}{2}\rho_I g w_I(1-2\phi)(\rho_W/\rho_I)\alpha_W \\ &= \bar{P}_I(w_I/h_I)[\phi\alpha + (1-2\phi)(\rho_W/\rho_I)\alpha_W]\end{aligned} \tag{26}$$

where $\Delta h/\Delta x \to \alpha$ and $\Delta h_W/\Delta x \to \alpha_W$ as $\Delta x \to 0$. Equation (26) is derived in Appendix A.

[35] Notice that if $\alpha_W = 0$, τ_O varies as $1 - \varphi$ and τ_S varies as φ, so a decrease in basal shear is replaced by a corresponding increase in side shear, and vice versa. However, in general, α_W is not zero. Equation (8) links α_W to φ:

$$\begin{aligned}\alpha_W &= \partial h_W/\partial x = (\rho_I/\rho_W)\partial(h_I\phi)/\partial x \\ &= (\rho_I/\rho_W)(\phi\alpha_I + h_I\partial\phi/\partial x)\end{aligned} \tag{27}$$

where $\alpha_I = \partial h_I/\partial x$ is the gradient of ice thickness. Substituting equation (27) for α_W in equations (25) and (26) gives

$$\begin{aligned}\tau_O &= P_I(1-\phi)[\alpha - (\rho_W/\rho_I)\alpha_W] \\ &= P_I(1-\phi)(\alpha - \phi\alpha_I - h_I\partial\phi/\partial x) \\ &= P_I(1-\phi)^2\alpha - P_I h_I(1-\phi)\partial\phi/\partial x\end{aligned} \tag{28}$$

$$\begin{aligned}\tau_S &= \bar{P}_I(w_I/h_I)[\phi\alpha + (1-2\phi)(\rho_W/\rho_I)\alpha_W] \\ &= \bar{P}_I(w_I/h_I)[\phi\alpha + (1-2\phi)(\phi\alpha_I + h_I\partial\phi/\partial x)] \\ &= P_I(w_I/h_I)\phi(1-\phi)\alpha + \bar{P}_I w_I(1-2\phi)\partial\phi/\partial x\end{aligned} \tag{29}$$

where $\alpha = \alpha_I$ for $\Delta h = \Delta h_I$ within each Δx step, $\tau_O = P_I\alpha$ and $\tau_S = 0$ when $\varphi = 0$, and $\tau_O = \tau_S = 0$ when $\varphi = 1$ because then $\alpha = (\rho_W/\rho_I)\alpha_W$. The maximum value of τ_S is reached when $\varphi = 0.5$ but an increase in φ is always accompanied by a decrease in τ_O relative to τ_S.

Table 1. Kinematic Stresses Linked to Floating Fraction $\phi = w_F/w_I$ of Ice and Longitudinal Gravitational Forces Numbered in Figure 7 for the Geometrical Force Balance

Stress	Formula	Equation Number in Text
Effective basal water pressure at x, from gravity force 3	$P_W^* = \rho_W g h_W$	(3)
Ice overburden pressure at x, from gravity force (1 + 2 + 3 + 4)	$P_I = \rho_I g h_I$	(2)
Upslope tensile stress at x, from gravity force 4:	$\sigma_T = \bar{P}_I(1 - \rho_I/\rho_W)\phi^2$	(17)
Downslope water pressure stress at x, from gravity force 3	$\sigma_W = \bar{P}_I(\rho_I/\rho_W)\phi^2$	(16)
Upslope flotation stress at x from gravity force (3 + 4)	$\sigma_F = \sigma_T + \sigma_W = \bar{P}_I\phi^2$	(15)
Longitudinal force balance at x from gravity force [(5 + 6 + 7 + 8) − (1 + 2 + 3 + 4)]	$P_I\alpha = \partial(\sigma_F h_I)/\partial x + \tau_O + 2\tau_S(h_I/w_I)$	(33)
Flotation force gradient at x from gravity force [(7 + 8) − (3 + 4)]	$\partial(\sigma_F h_I)/\partial x = P_I\phi(\phi\alpha_I + h_I\partial\phi/\partial x)$	(32)
Basal shear stress at x from gravity force (5–1)	$\tau_O = P_I(1-\phi)^2\alpha - P_I h_I(1-\phi)\partial\phi/\partial x$	(28)
Side shear stress at x from gravity force (6–2)	$\tau_S = P_I(w_I/h_I)\phi(1-\phi)\alpha + \bar{P}_I w_I(1-2\phi)\partial\phi/\partial x$	(29)
Average downslope basal shear stress to x from gravity force 1	$\bar{\tau}_O = \bar{P}_I w_I h_I(1-\phi)^2/(w_I x + A_R)$	(21)
Average downslope side shear stress to x from gravity force 2	$\bar{\tau}_S = P_I w_I h_I\phi(1-\phi)/(2\bar{h}_I x + 2L_S\bar{h}_S + C_R\bar{h}_R)$	(22)
Downslope compressive stress at x due to $\bar{\tau}_O$ and $\bar{\tau}_S$ along x and σ_W at $x = 0$	$\sigma_C = \bar{P}_I - \sigma_T = \bar{P}_I - \bar{P}_I(1-\rho_I/\rho_W)\phi^2$	(18)
First-order floating fraction of ice at x	$\phi = h_O/h_I$	(24)

[36] The change in longitudinal stresses along Δx is obtained from a longitudinal force balance in buoyant ice below h_F in Figure 7 (top). A negative tensile gravitational force change is flow band width w_I times the difference between triangular areas 8 and 4 in Figure 7 (bottom). It is balanced by positive tensile force change $w_I\Delta(\sigma_T h_I)$ along incremental length Δx. Summing these changing forces to zero, dividing by Δx, solving for $\Delta(\sigma_T h_I)/\Delta x = \partial(\sigma_T h_I)/\partial x$ as $\Delta x \rightarrow 0$, and using equation (27) for α_W gives

$$\begin{aligned}\partial(\sigma_T h_I)/\partial x &= \rho_I g h_I(1-\rho_I/\rho_W)\phi(\rho_W/\rho_I)\alpha_W \\ &= P_I(1-\rho_I/\rho_W)\phi(\phi\alpha_I + h_I\partial\phi/\partial x)\end{aligned} \quad (30)$$

where $\partial(\sigma_T h_I)/\partial x = 0$ when $\varphi = 0$ and $\partial(\sigma_T h_I)/\partial x = P_I(1 - \rho_I/\rho_W)\alpha_I$ when $\varphi = 1$. Similarly, a negative compressive gravitational force change is w_I times the difference between triangular areas 7 and 3 in Figure 7 (bottom). It is balanced by positive compressive force change $w_I\Delta(\sigma_W h_I)$ along Δx due to the change in basal water pressure. Summing these changing forces to zero, dividing by Δx, and letting $\Delta x \rightarrow 0$ gives

$$\partial(\sigma_W h_I)/\partial x = P_I\alpha_W = P_I(\rho_I/\rho_W)\phi(\phi\alpha_I + h_I\partial\phi/\partial x) \quad (31)$$

The sum of negative tensile and compressive gravitational force gradients gives the negative flotation gravitational force gradient due to change ΔP^*_W along Δx. It is w_I times the difference between triangular areas (7 + 8) and (3 + 4) along Δx. It is balanced by positive flotation force change $w_I\Delta(\sigma_F h_I)$ along Δx. Summing these changing forces to zero, dividing by Δx, and letting $\Delta x \rightarrow 0$ gives

$$\partial(\sigma_F h_I)/\partial x = P_I\phi(\phi\alpha_I + h_I\partial\phi/\partial x) \quad (32)$$

Equations (30) through (32) can also be obtained directly from equations (15) through (17).

[37] Finally, the negative longitudinal gravitational force change along Δx given by w_I times the difference in area between the two big triangles, (5 + 6 + 7 + 8) − (1 + 2 + 3 + 4), can be summed to zero with positive resisting forces $w_I\Delta(\sigma_F h_I) + \tau_O w_I\Delta x + 2\tau_S\bar{h}_I\Delta x$. Dividing by Δx and letting $\Delta x \rightarrow 0$ gives

$$P_I\alpha = \partial(\sigma_F h_I)/\partial x + \tau_O + 2\tau_S(h_I/w_I) \quad (33)$$

where $\sigma_F = \sigma_T + \sigma_W$. Equation (33) is also obtained from the equilibrium equations [see *Van der Veen*, 1999, p. 40], but without σ_W, so that $\sigma_F = \sigma_T$, and without σ_F, σ_T, σ_W, τ_O, and τ_S all being related to ice bed coupling through floating fraction φ of basal ice. Those relationships emerge only from the geometrical force balance.

[38] Relationships between floating fraction φ of ice and stresses that resist gravitational motion, as presented in this section, are summarized in Table 1, and most are derived geometrically in Appendix A.

[39] Stresses in Table 1 are for a flow band of constant width w_I that coincides with the approximate width of an ice stream. Shear stresses vanish down the centerline of an ice stream, which is the central flow line in the flow band. Without side shear, the longitudinal driving force due to gravity and represented by the shaded areas of the gravita-

tional triangles in Figure 6 changes by $\Delta(\frac{1}{2}P_I h_I - \frac{1}{2}P_W^* h_F)$ in incremental length Δx and is balanced by basal drag force $\tau_O\,\Delta x$. From equations (2), (3) and (8):

$$\tau_O \Delta x = \Delta\left(\frac{1}{2}P_I h_I - \frac{1}{2}P_W^* h_F\right) = \Delta\left(\frac{1}{2}P_I h_I - \frac{1}{2}P_I \phi h_I \phi\right)$$
$$= \rho_I g h_I (1-\phi^2)\Delta h_I - \rho_I g h_I^2 \phi \Delta\phi \qquad (34)$$

Setting $\alpha = \Delta h_I/\Delta x = \Delta h/\Delta x$ for ice columns having a horizontal base on steps of an up-down staircase bed, and solving for τ_O:

$$\tau_O = P_I(1-\phi^2)\alpha - P_I h_I \phi \Delta\phi/\Delta x \qquad (35)$$

Compare equation (35) with equation (28). The same procedure employed in equations (18) through (24), but excluding all terms for side shear, delivers equation (24) for the central flow line of a flow band. Hence, equation (10) applies to both flow bands and flow lines, so it is a robust result of the geometrical force balance.

[40] Figure 8 is a plot of normalized stresses τ_O, τ_S, σ_T, σ_F, σ_W, and σ_C for flow bands, and τ_O given by equation (35) for flow lines, versus φ. It shows how removing side shear stress τ_S in flow bands is compensated by increasing basal shear stress τ_O in flow lines at the center of flow bands. Since radar sounding is often along single flight lines down the centers of ice streams, Equation (35) for τ_O is preferred for the centerline bed profile. An identical resistance to gravitational forcing is entailed by using a flow line instead of a flow band. In Figure 8, normalized basal resistance represented by $\tau_O/P_I\alpha$ for a flow line is identical to the normalized resistance provided by the flow band for $\tau_O/P_I\alpha$ at the bed and $2(h_I/w_I)\tau_S/P_I\alpha$ along the two sides.

4. Applications

[41] The geometrical force balance, or any force balance, can give only first approximations to profiles for sheet, stream, and shelf flow because the mass balance is excluded from the analysis. This is illustrated in Figure 9, which compares profiles for ice sheets (top) and ice shelves (bottom). Figure 9 (top) shows that the parabolic ice sheet profiles obtained from equation (6) using only a force balance generally lies between elliptical profiles obtained from the flow law of ice (profile 1) and the sliding law of ice (profile 2), as required when a mass balance with a constant surface accumulation rate is included along with the force balance [*Hughes*, 1981, Figure 5.8]. Figure 9 (bottom) shows that the flat ice shelf profile consistent with equation (5) using only a force balance is comparable to the profile that also include the mass balance for a constant accumulation rate, except near the ice shelf grounding line where inflowing ice offsets the gravitational thinning and ice shelf stretching that is resisted by σ_T [see *Van der Veen*, 1999, Figure 6.10].

[42] Another comparison of results using only a force balance with results that combine the force balance and the mass balance is provided by the radar flight line down Byrd Glacier, Antarctica that provided a nearly continuous bed

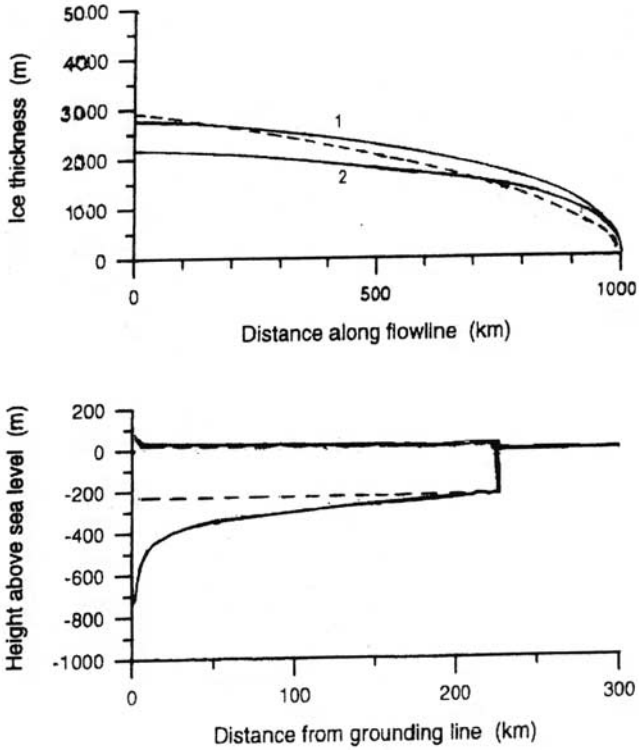

Figure 9. Comparing flow line profiles from the force balance with profiles from the force balance and the mass balance. (top) For sheet flow, a parabolic force balance profile (dashed curve) from equation (6) is compared with elliptical force/mass balance profiles obtained from the flow law (curve 1) and the sliding law (curve 2) of ice (modified from *Hughes* [1981, Figure 5.8]). (bottom) For shelf flow, force balance profiles (dashed lines with constant thickness) from equation (5), are compared with force/mass balance profiles obtained from the flow law for longitudinal tension (concave profile) (modified from *Van der Veen* [1999, Figure 6.10]).

reflection. As seen in Figure 10, the flight line is generally not too far from the central flow line. Figure 11 shows the surface and bed profiles along this flight line (Figure 11, top) and compares φ calculated by *Vance and Ashley* [2006] using equation (24) for the force balance with φ calculated by *Reusch and Hughes* [2003] using a combined force balance and mass balance (Figure 11, bottom). The trend in φ is the same in both cases, but φ from the force balance lies below φ from the combined balance, except for $\varphi = 1$ for floating ice beyond the (un)grounding line.

[43] These results, and the robust nature of equation (24) for both flow bands and flow lines, encourage using equation (24) to calculate $\varphi = h_O/h_I$ along straight-line approximations to Antarctic ice flow lines that enter major ice streams (see Figure 12). The straight-line approximations were provided by J. Fastook using BEDMAP data to obtain h_O at $x = 0$ and h_I along x for these flow lines in calculating φ along x. BEDMAP data are least reliable in Queen Maude Land, the northeast quadrant of Figure 12. High values of φ extend farthest up flow lines when the concave surface of ice streams extend farthest inland, such

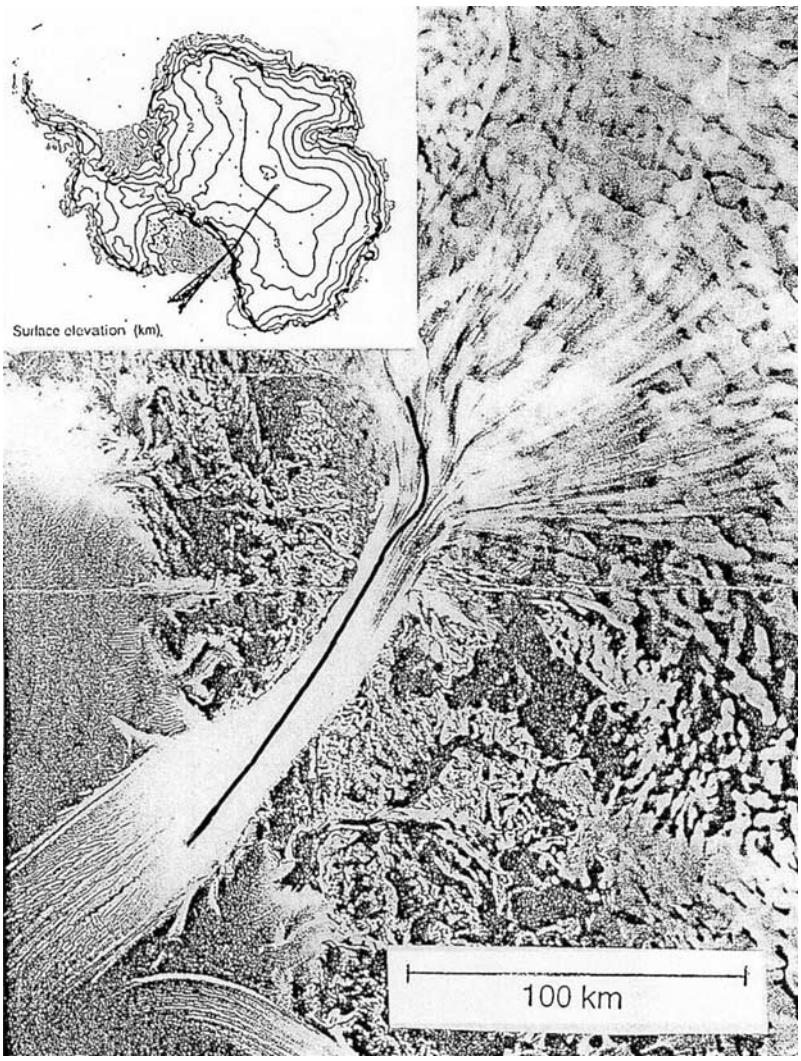

Figure 10. A radio echo flight line that is subparallel to a central ice flow band on Byrd Glacier, Antarctica. The Radarsat image is from *Jezek* [1998].

as along West Antarctic ice streams and up Lambert Glacier in East Antarctica.

[44] All three applications call attention to a problem in using equation (24) for φ. So long as h_O is finite at $x = 0$, equation (24) give a finite value of φ all along x clear to the interior ice divide of an ice sheet. However, as defined by equation (8), a frozen bed requires that $w_F/w_I = 0$ so that $\varphi = 0$. Therefore these two expressions for φ are incompatible when h_O is finite and the bed becomes frozen, and even when the bed remains thawed but φ is very low. In these cases $h_I = h_O/\varphi$ becomes unrealistically high for realistic value of h_O. My interpretation is that equation (24), being derived using only the force balance, does not apply for low φ values unless h_O is also low, just as constant basal shear stress τ_O in equation (6), also derived using only the force balance, does not deliver $\tau_O = 0$ at ice divides where $\alpha = 0$ (see equation (7)). Equation (8) gives the correct value of φ. The mass balance must be combined with the force balance before expressions allowing $\varphi = 0$ for a frozen bed can be derived when h_O is at an ice stream (un)grounding line. Obtaining $\tau_O = 0$ at ice divides where $\alpha = 0$, as shown in Figure 9 (top), requires combining the force and mass balance [*Hughes*, 1981].

5. Discussion and Conclusions

[45] The geometrical approach to the force balance delivers all the stresses for shelf flow and sheet flow that are delivered analytically by integrating the equilibrium equations. In addition, the geometrical approach also delivers the stresses for stream flow, and relates these stresses to a decrease of floating fraction φ up ice streams that give ice streams their characteristic concave surface profile. The geometrical approach is not an invention that the inventor can manipulate at will. It is a discovery, which I have explored for two decades, beginning in 1988. The initial discovery linked the "pulling power" of ice streams to a downstream increase in φ that progressively uncoupled ice from the bed [*Hughes*, 1992]. Table 1 links all important stresses in ice streams to floating fraction φ of ice. Only the geometrical force balance delivers this result. It is probably as far as a geometrical approach can go. The next level would be variable flow band widths, for which the geometry becomes unwieldy.

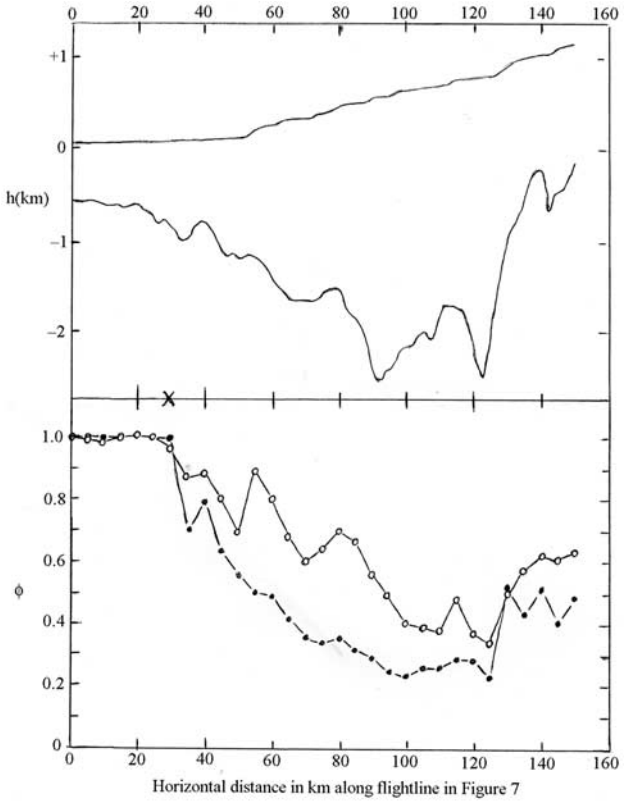

Figure 11. The floating fraction of basal ice along Byrd Glacier. (top) Surface (upper line) and basal (lower line) radar reflections along the flight line in Figure 10. (bottom) Taking the grounding line at x, variations of φ are shown from the study by *Reusch and Hughes* [2003] as connected circles and from equation (24) as connected dots (modified from *Vance and Ashley* [2006]).

[46] The initial discovery that the concave surface profile of an ice stream depends to a strong first approximation on ice bed coupling linked directly to the floating fraction φ of ice along the ice stream has, so far, led to seven conclusions.

[47] 1. The bed under an ice stream must consist of linked water-filled cavities on the lee side of bedrock steps [*Kamb*, 1987] or linked water-filled pockets incised in mobilized till [*Ng*, 2000], as discussed by *Hooke* [2005, pp. 216–230] and illustrated in Figure 13. Cavities are linked by orifices and pockets are linked by channels that control subglacial hydrology by opening and closing. When closed, cavities and pockets are isolated. When opened, water in the cavities and pockets leaks out, shrinking them, and thereby forcing bedrock or till to bear more of the ice overburden. *Engelhardt and Kamb* [1997] and *Kamb* [2001] reported that $P_W \approx 0.9\ P_I$ in dozens of core holes through Whillans and Kamb Ice Streams in West Antarctica, showing that some orifices and channels remain open all the way to the Ross Ice Shelf. The more w_F decreases compared to w_I, where $\varphi = w_F/w_I = P^*_W/P_I$ in equation (8), the more resistance the bed provides to horizontal ice motion. Again, $P_W \approx P_I$ in the vertical force balance, equation (2) and (3), but $0 < P^*_W/P_I < 1$ in the horizontal force balance, equations (8) and (9), for which P^*_W is an effective basal water pressure less than actual basal water pressure P_W. In the geometrical representation of the horizontal gravitational driving force, P^*_W is a pseudo basal water pressure that applies to the floating fraction $\varphi = w_F/w_I$ of ice.

[48] 2. Basal water must be produced at a rate that replaces water lost by leakage, otherwise cavities and pockets would close and the concave profile of streamflow would revert to the convex profile of sheet flow. That West Antarctic ice streams are known to turn on and off over time [*Anandakrishnan et al.*, 2001] indicates that this subglacial hydrological system is unstable. Therefore, floating fraction φ at any location along an ice stream is determined by all downstream processes that can open or close orifices and channels. These processes ultimately depend on variations in basal drag, whether under ice streams or under ice ridges between ice streams that give rise to side drag in ice streams, or in confined ice shelves, or under ice lobes. *Raymond et al.* [2001] showed how instabilities in side drag are linked to instabilities in basal drag. The wider an ice stream, the less important side drag becomes (see equation (29)).

[49] 3. In a longitudinal geometrical force balance applied to ice streams, the downstream gravitational driving force for a given flow band width is the area $\frac{1}{2}P_I h_I$ of a triangle having base P_I and height h_I. Resisting forces can be assigned to specific portions of this triangle. Two portions, the white areas $\frac{1}{2}P^*_W h_F$ of gravitational triangles in Figure 6, are equated with resistance assigned to floating ice. Area $\frac{1}{2}P^*_W h_W$ is a back force that resists stream flow, with downstream compression all along x determining φ at x in the ice stream. Area $\frac{1}{2}P^*_W(h_F - h_W)$, with ice height h_F floated by water height h_W, is an upstream tensile force at x. Two portions, the shaded areas $\frac{1}{2}P_I h_I - \frac{1}{2}P^*_W h_F$ of the gravitational triangles in Figure 6, are equated with resistance assigned to grounded ice. These shaded areas are partitioned between basal and side shear by linking basal shear to the shaded triangles above h_F and side shear to the shaded parallelograms below h_F. Area $\frac{1}{2}(P_I - P^*_W)(h_I - h_F)$ above h_F is a back force caused by basal shear. Area $(P_I - P^*_W)\ h_F$ below h_F is a back force caused by side shear. These four resisting forces add to give area $\frac{1}{2}P_I h_I$ for the downstream gravitational driving force. Then only basal drag remains when $\varphi = 0$ for pure sheet flow, basal and side drag exist when $0 < \varphi < 1$ for stream flow, and basal and side drag vanish when $\varphi = 1$ for unconfined shelf flow. These conditions are met only by partitioning triangle $\frac{1}{2}P_I h_I$ for the gravitational driving force as shown in Figures 6 and 7. No other possibilities exist that allow smooth transitions in surface profiles for sheet, stream, and shelf flow. This partitioning of gravitational driving force $\frac{1}{2}P_I h_I$ gives rise to resisting longitudinal tensile and compression stresses σ_T and σ_W in the floating part of stream flow, and basal and side shear stresses τ_O and τ_S in the grounded part.

[50] 4. Variations in φ that reflect changes in the size and distribution of linked water cavities and water pockets in bedrock and till, respectively, under ice streams can be monitored by changes in effective height h_W of water compared to ice height h_I above the bed in Figure 6. This ratio is tied to width ratio w_F/w_I for ice "floating" above water cavities and pockets compared to total flow band width w_I such that $\phi = (\rho_W/\rho_I)h_W/h_I = h_F/h_I = w_F/w_I$ in equation (8), where $h_F = (\rho_W/\rho_I)h_W$ is the height of ice that would just float in water of height h_W. This relationship gives rise to a longitudinal stress σ_W acting across h_I according to a longitudinal force balance $\sigma_W h_I = \bar{P}^*_W h_W$

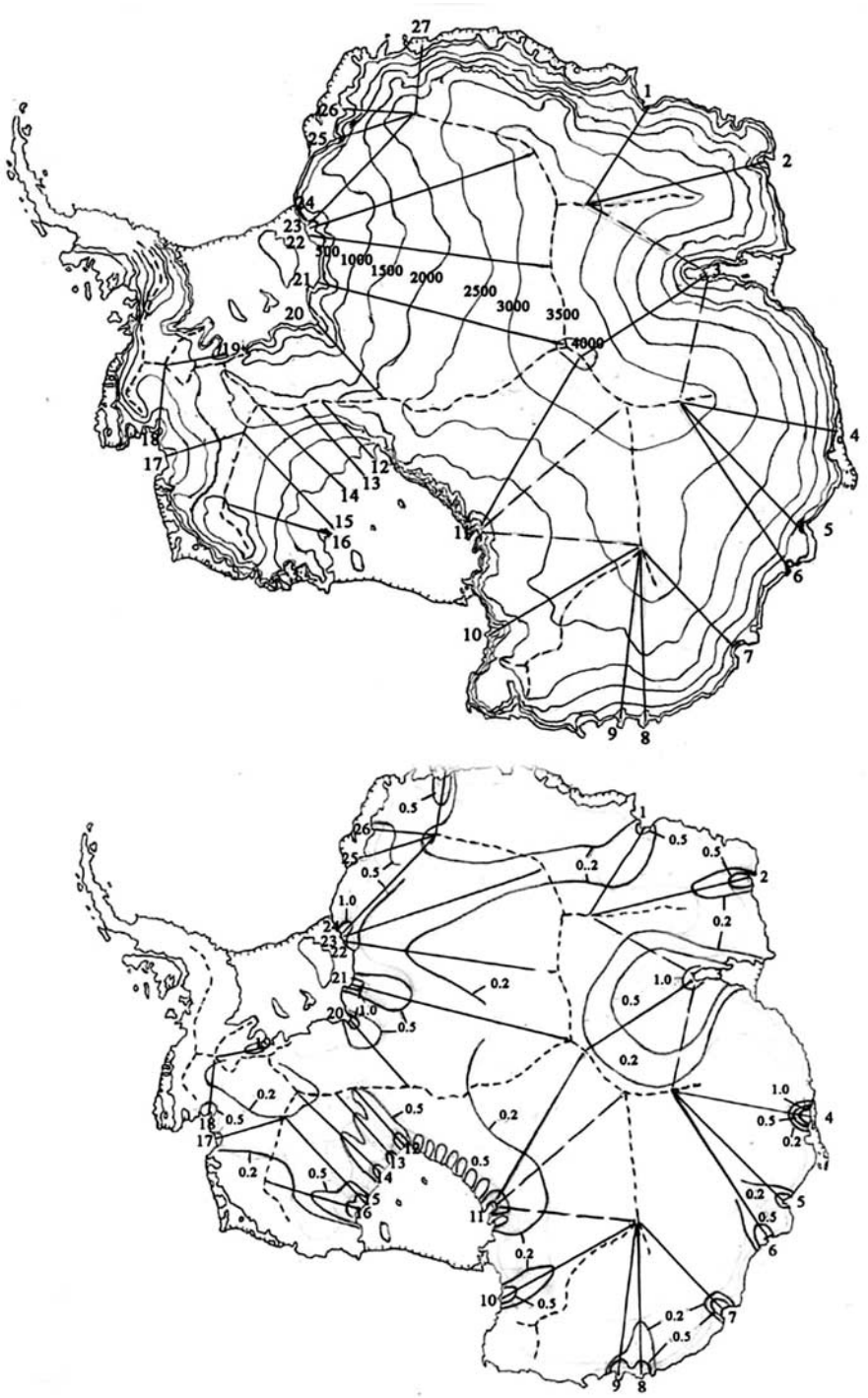

Figure 12. The floating fraction of basal ice for Antarctic ice stream flow lines approximated by straight lines. (top) Ice surface elevations, 500 m contours. (bottom) Floating fraction $\varphi = h_O/h_I$ given by equation (24).

that is understood most clearly at an ice shelf calving front where $\bar{P}^*_W = \bar{P}_W$ (see Figure 6, top) but applies all along an ice stream. This force balance applies from the calving front to the grounding line of the ice shelf and up the ice stream to produce its concave profile so long as w_F/w_I decreases slowly, whereas it produces convex profiles up ice ridges when w_F/w_I decreases rapidly (see Figure 4).

[51] 5. A confined and pinned ice shelf (shown in Figure 7) contributes to φ at any location up the ice stream supplying the ice shelf. Confinement generates shear stresses along side grounding lines. Basal pinning generates basal shear across ice rumples and side shear around ice rises. All are treated in equations (18) through (23) leading to equation (24) for φ. For ice rises, back force $F_B = \bar{\tau}_S \bar{h}_R C_R$, where mean shear stress $\bar{\tau}_S$ around an ice rise of circumference C_R and mean ice thickness $\bar{h}_R$, is equivalent to back force $F_B = 2\bar{\tau}_S \bar{h}_R D_L + (\bar{\sigma}_C + \bar{\sigma}_T)\bar{h}_R D_T$, where D_L and D_T are longitudinal and transverse diameters of the ice rise, $\bar{\sigma}_C$ is the mean compressive stress on its stoss side, and $\bar{\sigma}_T$ is the mean tensile stress on its lee side. Both cause transverse shear.

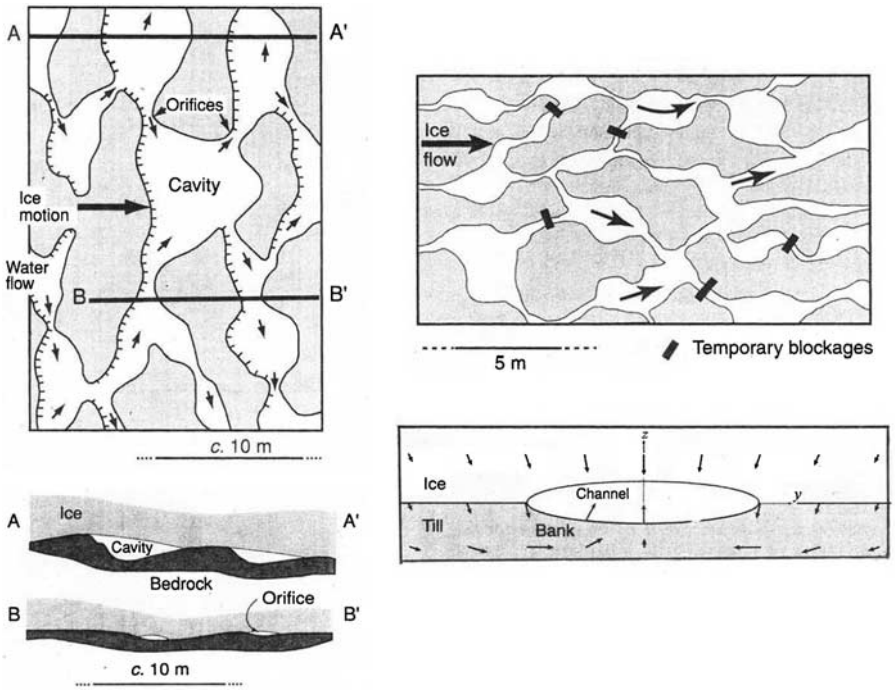

Figure 13. Determining floating fraction φ of ice in the force balance along ice streams. Basal conditions shown allow variations $0 \leq \varphi \leq 1$ with $\varphi \approx 0$ where ice contacts the bed (gray areas) and $\varphi \approx 1$ where ice contacts only basal water (white areas). (left) Water flow (arrows) for a linked water cavity basal water system on jointed bedrock. (right) Water flow (arrows) for a linked water pocket basal water system on till. (top) These systems in the map plane. (bottom) Cross sections of orifices that connect water cavities (left) and channels that connect water pockets (right). Compiled from *Hooke* [2005, Figures 8.14, 8.20, and 8.22] and reproduced with permission.

[52] 6. A marine ice stream supplying a floating ice shelf becomes a terrestrial ice stream supplying a grounded ice lobe of length x in equations (18) through (23) by setting $L_S = C_R = 0$ and expanding A_R to be the entire basal area of the ice lobe. Then $A_R = w_I x$ and equation (6) gives a parabolic convex lobe profile for constant τ_O. There is nothing inherent in h_W shown in Figure 6 that prevents the geometrical force balance from being applied to both marine and terrestrial ice streams, once the proper meaning of $\phi = (\rho_W/\rho_I)h_W/h_I = h_F/h_I = w_F/w_I$ in equation (8) is understood. Pooling and leakage of basal water, which determines φ, can be treated independently of whether an ice stream ends in water or on land [see *Weertman*, 1972; *Weertman and Birchfield*, 1982; *Tulaczyk et al.*, 2000a, 2000b; *Johnson and Fastook*, 2002; *Christoffersen and Tulaczyk*, 2003].

[53] 7. Floating fraction φ of ice is a somewhat elusive quantity. As defined by equation (8), local resistance to longitudinal ice motion gives $\varphi = w_F/w_I$ in which "floating" width w_F of flow band width w_I can include saturated till that has no resistance to ice motion [*Kamb*, 1991] in addition to the water-filled cavities and pockets in Figure 13. As defined by equation (10) and then derived to obtain equation (24), the value of φ in equation (8) also depends on $\varphi = h_O/h_I$ such that h_O is where a marine ice stream becomes a floating tongue or ice shelf ($h_O = h_I$) and where a terrestrial ice stream becomes a grounded ice lobe ($h_O \rightarrow h_I$). Equating equations (8) and (10) gives $w_F/w_I = h_O/h_I$ so that w_F locally in an ice stream depends on a downstream location where $h_O \approx h_I$ and h_O depends on buttressing by water and by a confined and/or pinned ice shelf for a marine ice stream and on buttressing by an ice lobe for a terrestrial ice stream. The less buttressing, the lower h_O will be and therefore the lower h_I will be upstream. In making these distinctions, $h_F = h_W(\rho_W/\rho_I) = P^*_W/\rho_I g = h_I(w_F/w_I)$ in equations (8) and (9) is a purely mathematical (not physical) quantity that allows the relationship $w_F/w_I = h_O/h_I$ to be obtained from the geometry of a longitudinal force balance in ice streams as shown in Figure 7. The inescapable conclusion is that subglacial hydrology is the mechanism that links w_F locally to h_O downstream. Quantifying this linkage in terms of physical processes then emerges as a major task in glaciology.

[54] 8. The eighth and most important conclusion is $\varphi = h_O/h_I$ proposed in equation (10) as a first-order approximation for both marine and terrestrial ice streams. The derivation of equation (10) included the back force from a confined and pinned ice shelf beyond a marine ice stream. Ice shelf buttressing is represented by h_O in equation (10). The more buttressing, the higher ice height $h = h_O(1 - \rho_I/\rho_W)$ must float above water to provide the gravitational driving force needed to balance the buttressing force at the grounding line where $\varphi = 1$. For a terrestrial ice stream, the buttressing force is supplied by a terminal ice lobe grounded on land, with h_O at the upper end of the ice lobe where $\varphi \rightarrow 1$. Equation (10) forces glaciologists to confront the fact that, without the mass balance, the force balance alone can convert high convex ice sheets, for which $\varphi = 0$, into their configuration of minimal potential energy, a low flat ice shelf for which $\varphi = 1$, merely by increasing φ along flow. This requires converting potential energy into kinetic (and

thermal) energy. The proper niche for ice in the density-based stratigraphic layering of Earth's constituents is between the ocean and the atmosphere, not the land and the atmosphere. The mass balance keeps ice sheets on land. Equation (10), applied along flow, shows in a first-order way how far along this journey from land (grounded) to sea (floating) an ice sheet is, as illustrated in Figure 12 for the Antarctic Ice Sheet. This journey is also a journey of the mind. It requires thinking outside the box. For those who make the journey, glaciology will never be the same again. Equation (10) is the vehicle on this journey. At the end of the journey, ice sheets are seen as the only component of Earth's climate machine that can destroy itself and can therefore terminate a Quaternary glaciation cycle. These cycles end abruptly, as terminations.

[55] The eight conclusions discussed above require a measure of faith in the geometrical force balance. There are no rigorous "proofs" for any of them. Neither can they be disproven. If they are accepted, then the expressions linking resisting stresses to φ in Table 1 are correct. These stresses apply for flow band models. Would they also apply to grid point models that treat flow in the map plane if the force balance and mass balance are combined? Can time-dependent ice thinning or thickening rates be determined from perturbations in φ? Answers to these and other questions must await general acceptance of the geometrical force balance.

Appendix A: Relating φ to Stresses Using Gravitational Geometry

[56] Areas of triangles and parallelograms are as follows:

[57] At x,

$$ADF = 1/2AD\cdot DF = 1/2h_I\cdot P_I = 1/2h_I\cdot\rho_I g h_I = 1/2\rho_I g h_I^2$$

$$BDE = 1/2BD\cdot DE = 1/2h_F\cdot P_W^* = 1/2h_I\phi\cdot\rho_I g h_I\phi = 1/2\rho_I g h_I^2\phi^2$$

$$CDE = 1/2CD\cdot DE = 1/2h_W\cdot P_W^* = 1/2h_I(\rho_I/\rho_W)\phi\cdot\rho_I g h_I\phi$$
$$= 1/2\rho_I g h_I^2(\rho_I/\rho_W)\phi^2$$

$$BCE = 1/2BD\cdot CH = 1/2h_F\cdot\rho_I g(h_F - h_W)$$
$$= 1/2\rho_I g h_I^2(1-\rho_I/\rho_W)\phi^2$$

$$ABG = 1/2AB\cdot BG = 1/2(h_I - h_F)\cdot\rho_I g(h_I - h_F)$$
$$= 1/2\rho_I g h_I^2(1-\phi)^2$$

$$BEFG = BD\cdot BG = h_F\cdot\rho_I g(h_I - h_F) = \rho_I g h_I^2\phi(1-\phi)$$

[58] At $x + \Delta x$,

$$A'D'F' = 1/2A'D'\cdot D'F' = 1/2(h_I+\Delta h)\cdot(P_I+\Delta P_I)$$
$$= 1/2(h_I+\Delta h)\cdot\rho_I g(h_I+\Delta h)$$

$$B'D'E' = 1/2B'D'\cdot D'E' = 1/2(h_F+\Delta h_F)\cdot\left(P_W^*+\Delta P_W^*\right)$$
$$= 1/2(h_F+\Delta h_F)\cdot\rho_I g(h_W+\Delta h_W)$$

$$C'D'E' = 1/2C'D'\cdot D'E' = 1/2(h_W+\Delta h_W)\cdot\left(P_W^*+\Delta P_W^*\right)$$
$$= 1/2(h_W+\Delta h_W)\cdot\rho_I g(h_W+\Delta h_W)$$

$$B'C'E' = 1/2B'D'\cdot C'H' = 1/2(h_F+\Delta h_F)\cdot\rho_I g[(h_F+\Delta h_F) - (h_W+\Delta h_W)]$$

$$A'B'G' = 1/2A'B'\cdot B'G' = 1/2[(h_I+\Delta h_I)-(h_F+\Delta h_F)]\cdot\rho_I g[(h_I+\Delta h_I)-(h_F+\Delta h_F)]$$

$$B'E'F'G' = B'D'\cdot B'G' = (h_F+\Delta h_F)\cdot\rho_I g[(h_I+\Delta h_I)-(h_F+\Delta h_F)]$$

[59] Incremental changes in incremental length Δx are

$$\Delta h_W = (\rho_I/\rho_W)\Delta(h_I\phi) = (\rho_I/\rho_W)(h_I\Delta\phi + \phi\Delta h_I)$$
$$\Delta h_F = (\rho_W/\rho_I)\Delta h_W = \Delta(h_I\phi) = h_I\Delta\phi + \phi\Delta h_I$$

[60] Calculating stresses from $\sum F_x = F_G - F_R = 0$.

[61] Calculate σ_T from triangle area BCE.

$$F_R = \sigma_T h_I w_I = -F_G = (BCE)w_I$$
$$= \left[1/2\rho_I g h_I^2(1-\rho_I/\rho_W)\phi^2\right]w_I$$
$$\sigma_T = 1/2\rho_I g h_I(1-\rho_I/\rho_W)\phi^2 = \bar{P}_I(1-\rho_I/\rho_W)\phi^2$$

[62] Calculate σ_C from triangle areas $ADF-BCE$.

$$F_R = \sigma_C h_I w_I = F_G = (ADF - BCE)w_I$$
$$= \left[1/2\rho_I g h_I^2 - 1/2\rho_I g h_I^2(1-\rho_I/\rho_W)\phi^2\right]w_I$$
$$\sigma_C = 1/2\rho_I g h_I\left[1-(1-\rho_I/\rho_W)\phi^2\right] = \bar{P}_I\left[1-(1-\rho_I/\rho_W)\phi^2\right]$$

[63] Calculate $\bar{\tau}_O$ from triangle are ABG.

$$F_R = \bar{\tau}_O(w_I x + A_R) = F_G = (ABG)w_I$$
$$= \left[1/2\rho_I g h_I^2(1-\phi)^2\right]w_I$$
$$\bar{\tau}_O = 1/2\rho_I g h_I^2(1-\phi)^2 w_I/(w_I x + A_R)$$
$$= \bar{P}_I h_I w_I(1-\phi)^2/(w_I x + A_R)$$

[64] Calculate $\bar{\tau}_S$ from parallelogram area $BEFG$.

$$F_R = \bar{\tau}_S\left(2\bar{h}_I x + 2\bar{h}_S L_S + \bar{h}_R C_R\right) = F_G$$
$$= (BEFG)w_I = \left[\rho_I g h_I^2\phi(1-\phi)\right]w_I$$
$$\bar{\tau}_S = \rho g h_I^2\phi(1-\phi)w_I/\left(2\bar{h}_I x + 2\bar{h}_S L_S + \bar{h}_R C_R\right)$$
$$= P_I h_I w_I\phi(1-\phi)/\left(2\bar{h}_I x + 2\bar{h}_S L_S + \bar{h}_R C_R\right)$$

[65] Calculate τ_O from triangular areas $A'B'G'-ABG$.

$$F_R = \tau_O w_I\Delta x = F_G = (A'B'G' - ABG)w_I$$
$$\tau_O\Delta x = A'B'G' - ABG = \Delta(ABG)$$
$$= 1/2\rho_I g\Delta\left[h_I^2(1-\phi)^2\right]$$
$$= 1/2\rho_I g\left[h_I^2\Delta(1-\phi)^2 + (1-\phi)^2\Delta h_I^2\right]$$
$$= \rho_I g\left[h_I^2(1-\phi)\Delta(1-\phi) + (1-\phi)^2 h_I\Delta h_I\right]$$
$$= \rho_I g h_I(1-\phi)(\Delta h_I - h_I\Delta\phi - \phi\Delta h_I)$$
$$\tau_O = P_I(1-\phi)[\Delta h_I/\Delta x - \Delta(h_I\phi)/\Delta x]$$

[66] Calculate τ_S from parallelogram areas $B'E'F'G'-BEFG$.

$$F_R = 2\tau_S h_I\Delta x = F_G = (B'E'F'G' - BEFG)w_I$$
$$2\tau_S(h_I/w_I)\Delta x = B'E'F'G' - BEFG = \Delta(BEFG)$$
$$= \rho_I g\Delta\left[h_I^2\phi(1-\phi)\right]$$
$$= \rho_I g\left[h_I^2\phi\Delta(1-\phi) + h_I^2(1-\phi)\Delta\phi + \phi(1-\phi)\Delta h_I^2\right]$$
$$= \rho_I g\left[h_I^2\phi(-\Delta\phi) + h_I^2(1-\phi)\Delta\phi + \phi(1-\phi)(2h_I\Delta h_I)\right]$$
$$= \rho_I g h_I[\phi\Delta h_I + (h_I\Delta\phi + \phi\Delta h_I) - 2\phi(h_I\Delta\phi + \phi\Delta h_I)]$$
$$= \rho_I g h_I[\phi\Delta h_I + (1-2\phi)(h_I\Delta\phi + \phi\Delta h_I)]$$
$$\tau_S = \bar{P}_I(w_I/h_I)[\phi\Delta h_I/\Delta x + (1-2\phi)\Delta(h_I\phi)/\Delta x]$$

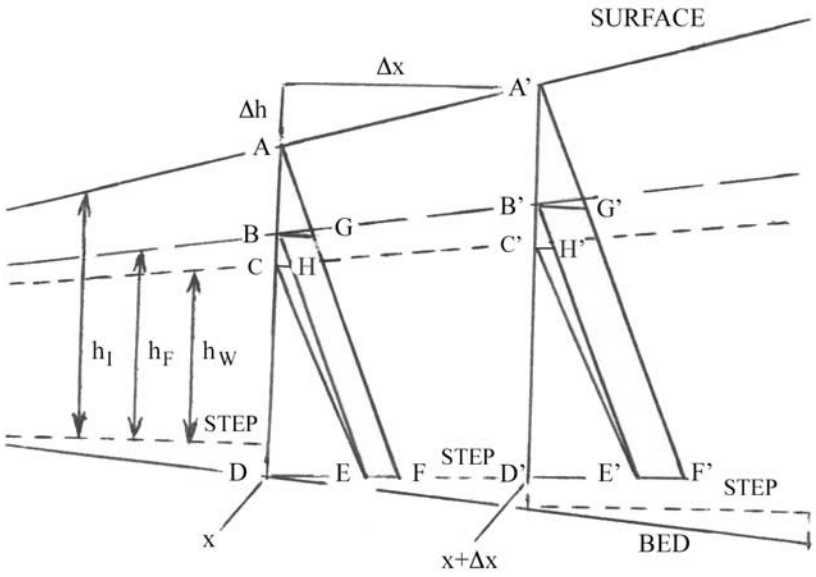

Figure A1. Gravitational forces along x represented geometrically.

[67] Longitudinal force balance in incremental length Δx of flow band $\Delta h_I = \Delta h + \Delta h_B = \Delta h$ for an ice column with a horizontal base.

[68] Balance forces over Δx for the ice column of width w_I.

$$\begin{aligned}
\sum F_x &= F_G - F_R = 0\\
F_R &= (\sigma_F + \Delta\sigma_F)(h_I + \Delta h_I)w_I - \sigma_F h_I w_I\\
&\quad + \tau_O w_I \Delta x + 2\tau_S(h_I + 1/2\Delta h_I)\Delta x\\
&= (\sigma_F h_I + \sigma_F \Delta h_I + h_I \Delta\sigma_F + \Delta\sigma_F \Delta h_I - \sigma_F h_I)w_I\\
&\quad + [\tau_O w_I + 2\tau_S(h_I + 1/2\Delta h_I)]\Delta x\\
&= [\Delta(\sigma_F h_I) + \Delta\sigma_F \Delta h_I]w_I + [\tau_O w_I + 2\tau_S h_I + \tau_S \Delta h_I]\Delta x\\
F_G &= [1/2(P_I + \Delta P_I)(h_I + \Delta h)w_I - 1/2 P_I h_I w_I]\\
&= 1/2(P_I \Delta h + h_I \Delta P_I + \Delta P_I \Delta h)w_I\\
&= 1/2[(\rho_I g h_I)\Delta h + h_I(\rho_I g \Delta h) + (\rho_I g \Delta h)\Delta h]w_I\\
&= (\rho_I g h_I \Delta h + 1/2\rho_I g \Delta h \Delta h)w_I\\
F_R = F_G &= [\Delta(\sigma_F h_I) + \Delta\sigma_F \Delta h_I]w_I + [\tau_O w_I + 2\tau_S h_I + \tau_S \Delta h_I]\Delta x\\
&= [\rho_I g h_I \Delta h + 1/2\rho_I g \Delta h \Delta h]w_I
\end{aligned}$$

[69] Solving for $\rho_I g h_I \Delta h/\Delta x$,

$$\begin{aligned}
\rho_I g h_I \Delta h &= \Delta(\sigma_F h_I) + \Delta\sigma_F \Delta h_I + \tau_O \Delta x\\
&\quad + (\tau_S/w_I)(2h_I + \Delta h_I)\Delta x\\
&\quad - 1/2\rho_I g \Delta h \Delta h\\
\rho_I g h_I(\Delta h/\Delta x) &= \Delta(\sigma_F h_I)/\Delta x + \Delta\sigma_F(\Delta h_I/\Delta x) + \tau_O\\
&\quad + (\tau_S/w_I)(2h_I + \Delta h_I) - 1/2\rho_I g \Delta h(\Delta h/\Delta x)
\end{aligned}$$

$$\begin{aligned}
\text{As } \Delta x \to 0, \Delta\sigma_F &\to 0, \Delta h \to 0, \Delta h/\Delta x\\
&\to \alpha, \Delta h_I/\Delta x \to \alpha_I, \text{and} \Delta(\sigma_F h_I)/\Delta x\\
&\to \partial(\sigma_F h_I)/\partial x \text{ as } \Delta x \to 0,
\end{aligned}$$

so

$$\rho_I g h_I \alpha = \partial(\sigma_F h_I)/\partial x + \tau_O + 2\tau_S(h_I/w_I)$$

[70] Here longitudinal flotation stress $\sigma_F = \sigma_W + \sigma_T$ results from floating ice below $h_F = h_W(\rho_W/\rho_I)$ in contact only with basal water, whereas shear stresses τ_O and τ_S result from shearing flow of ice in contact with solid boundaries at the bed and sides of the flow band, respectively.

[71] Check solutions for internal consistency.

[72] Solutions:

$$\begin{aligned}
\tau_O &= \rho_I g h_I[1 - \phi][\alpha - (\rho_W/\rho_I)\alpha_W]\\
\tau_S &= 1/2\rho_I g w_I \phi\alpha + 1/2\rho_I g w_I(1 - 2\phi)(\rho_W/\rho_I)\alpha_W\\
\partial(\sigma_F h_I)/\partial x &= \rho_I g h_I \phi(\rho_W/\rho_I)\alpha_W\\
\rho_I g h_I \alpha &= \partial(\sigma_F h_I)/\partial x + \tau_O + 2\tau_S(h_I/w_I)
\end{aligned}$$

[73] Substitute solutions for $\partial(\sigma_F h_I)/\partial x$, τ_O, and τ_S, and solve for α.

$$\begin{aligned}
\alpha &= \frac{\tau_O}{\rho_I g h_I} + \frac{2\tau_S}{\rho_I g w_I} + \frac{\partial(\sigma_F h_I)/\partial x}{\rho_I g h_I}\\
\alpha &= [1 - \phi][\alpha - (\rho_W/\rho_I)\alpha_W] + \phi\alpha + [1 - 2\phi](\rho_W/\rho_I)\alpha_W\\
&\quad + \phi(\rho_W/\rho_I)\alpha_W\\
&= \alpha + [\phi - 1](\rho_W/\rho_I)\alpha_W + [1 - 2\phi](\rho_W/\rho_I)\alpha_W\\
&\quad + \phi(\rho_W/\rho_I)\alpha_W\\
&= \alpha + [\phi - 1 + 1 - 2\phi + \phi](\rho_W/\rho_I)\alpha_W\\
&= \alpha
\end{aligned}$$

This appendix shows how all stresses are geometrically linked to ϕ using Figures A1 and A2.

Notation

- ϕ floating fraction of ice, equal to $P^*_W/P_I = \rho_W h_W/\rho_I h_I = h_W(\rho_W/\rho_I)/h_I = h_F/h_I = w_F/w_I$.
- g gravity acceleration.
- ρ_I ice density.
- ρ_W water density.
- h_I ice height above base giving P_I at base.
- h_W effective water height above base giving P^*_W at base, equal to $h_I(\rho_I/\rho_W)\phi$.

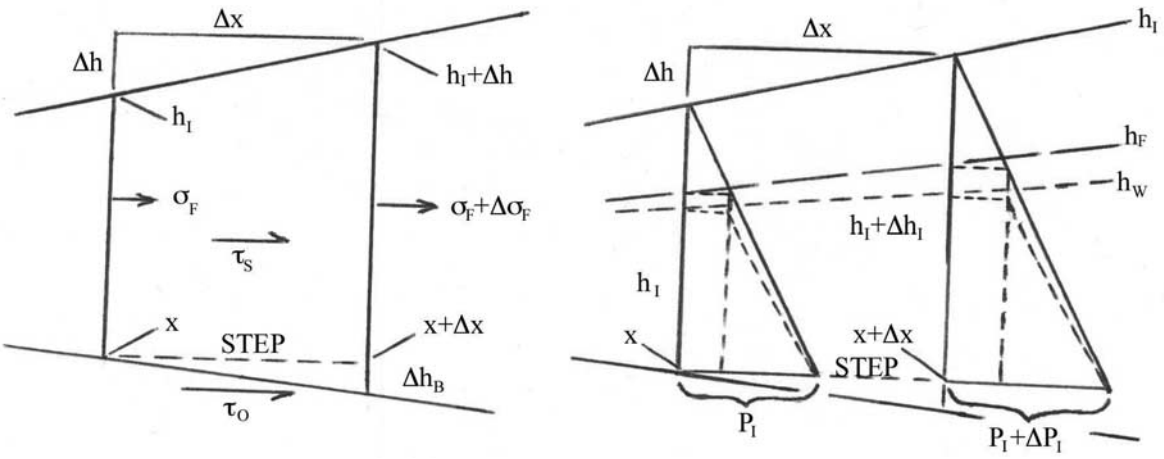

Figure A2. Horizontal forces in incremental length Δx of flow band.

P_I basal ice pressure averaged across flow band width w_I, equal to $\rho_I g h_I$.
P^*_W effective basal water pressure averaged across w_I, equal to $\rho_W g h_W = \rho_I g h_I \phi$.
h_F effective flotation ice height above base supported by P^*_W, equal to $h_W(\rho_W/\rho_I) = h_I\phi$.
w_I width of a flow band between adjacent flow lines on the ice surface.
w_F portion of w_I where basal water drowns bedrock or till.
h ice elevation above sea level in vertical direction z.
h_B bed height above (positive) or depth below (negative) sea level.
Δx incremental change in flow band length at the horizontal base of an ice column.
Δh incremental change in ice column elevation and thickness over Δx, equal to Δh_I.
Δh_B incremental change in bed elevation between Δx steps.
Δh_I ice thickness change between Δx steps, equal to $\Delta h - \Delta h_B$.
$\bar{h}_I$ mean ice thickness along distance x from ice shelf grounding line.
L_S length of ice shelf grounded along parallel flow band sides.
A_R area of ice shelf grounding at ice rumples within the flow band.
C_R circumference of ice shelf grounding around ice rises.
$\bar{h}_R$ mean ice thickness around ice rises.
F_G gravity force causing motion along x.
F_R resisting force resisting motion along x.
$\sum F_x$ sum of forces along x, equal to $F_G - F_R = 0$.

[74] **Acknowledgments.** The foundation for this work was laid in preparation for a 2-week glaciology course taught in June 2006 at Elizabeth City State University (ECSU) in North Carolina to black students interested in science and technology. Undergraduate students Keila Vance and Shrae Ashley from Jackson State University in Mississippi and Jarvis Bible College in Texas, respectively, applied equation (24) to calculate φ for Byrd Glacier, Antarctica, as shown in Figure 11. ECSU graduate student Kevin Jones applied equation (24) to calculate φ along 27 Antarctic flow lines entering major ice streams, as shown Figure 12. James Fastook at the University of Maine provided surface and bed topography along these flow lines using the BEDMAP program. JGR Associate Editor Johannes Weertman made suggestions that clarified and focused this work considerably. Four referees identified numerous problems needing clarification but also provided encouragement. In particular, Robert Thomas and Olga Sergienko provided several pages of detailed comments. Beverly Hughes delivered all versions of this work in numerous revisions. This work was supported by NASA and by NSF through the Center for Remote Sensing of Ice Sheets (CReSIS) at the University of Kansas, which helped to initiate the glaciology course at ECSU as part of its minority outreach program. I thank Linda Hayden and Malcolm LeCompte at ECSU for major assistance in this effort. The students presented their results at the Thirteenth Annual Workshop of the West Antarctic Ice Sheet Initiative (WAIS), sponsored by NSF, in 2006.

References

Anandakrishnan, S., et al. (2001), The flow regime of Ice Stream C and hypotheses concerning its recent stagnation, in *The West Antarctic Ice Sheet: Behavior and Environment*, *Antarct. Res. Ser.*, vol. 77, edited by R. B. Alley and R. A. Bindschadler, pp. 283–294, AGU, Washington, D. C.

Bader, H. (1961), The Greenland Ice Sheet, Monogr. 1-B2, 18 pp., U.S. Army Cold Reg. Sci. and Eng. Lab., Hanover, N. H.

Budd, W. F., et al. (1971), Derived physical characteristics of the Antarctic Ice Sheet, *Aust. Natl. Antarct. Res. Exped. (ANARE) Interim Rep., Ser. A (IV), Glaciol. Publ. 120*, 178 pp., Meteorol. Dep., Univ. of Melbourne, Melbourne, Australia.

Christoffersen, P., and S. M. Tulaczyk (2003), Thermodynamics of basal freeze-on: Predicting basal and subglacial signatures of stopped ice streams and interstream ridges, *Ann. Glaciol.*, *36*, 233–243, doi:10.3189/172756403781816211.

Dupont, T., and R. B. Alley (2005), Assessment of the importance of ice-shelf buttressing to ice-sheet flow, *Geophys. Res. Lett.*, *32*, L04503, doi:10.1029/2004GL022024.

Dupont, T. K., and R. B. Alley (2006), Role of small ice shelves in sea-level rise, *Geophys. Res. Lett.*, *33*, L09503, doi:10.1029/2005GL025665.

Engelhardt, H., and B. Kamb (1997), Basal hydraulic system of a West Antarctic ice stream: Constraints from borehole observations, *J. Glaciol.*, *43*, 207–230.

Glen, J. W. (1955), The creep of polycrystalline ice, *Proc. R. Soc. London, Ser. A*, *228*, 519–538, doi:10.1098/rspa.1955.0066.

Haefeli, R. (1961), Contribution to the movement and the form of ice sheets in the Arctic and Antarctic, *J. Glaciol.*, *3*, 1133–1150.

Hindmarsh, R. C. A. (2004), A numerical comparison of approximations to the Stokes equations used in ice sheet and glacier modeling, *J. Geophys. Res.*, *109*, F01012, doi:10.1029/2003JF000065.

Hooke, R. L. (2005), *Principles of Glacier Mechanics*, 2nd ed., 429 pp., Cambridge Univ. Press, Cambridge, U.K.

Hughes, T. J. (1981), Numerical reconstructions of paleo ice sheets, in *The Last Great Ice Sheets*, edited by G. H. Denton and T. Hughes, pp. 221–261, Wiley-Interscience, New York.

Hughes, T. (1992), On the pulling power of ice streams, *J. Glaciol.*, *38*, 125–151.

Hughes, T. (1998), *Ice Sheets*, 343 pp., Oxford Univ. Press, New York.

Hughes, T. (2003), Geometrical force balance in glaciology, *J. Geophys. Res.*, *108*(B11), 2526, doi:10.1029/2003JB002557.

Huybrechts, P. (1990), A 3-D model for the Antarctic Ice Sheet: A sensitivity study on the glacial-interglacial contrast, *Clim. Dyn.*, *5*, 79–92.

Jezek, K. C. (Ed.) (1998), Early results from the first RADARSAT-1 Antarctic mapping mission, *Tech. Rep. 98-02*, 22 pp., Byrd Pol. Res. Cent., Ohio State Univ., Columbus.

Johnson, J., and J. L. Fastook (2002), Northern Hemisphere glaciation and its sensitivity to basal melt water, *Quat. Int.*, *95–96*, 65–74, doi:10.1016/S1040-6182(02)00028-9.

Kamb, B. (1987), Glacier surge mechanism based on linked cavity configuration of the basal water conduit system, *J. Geophys. Res.*, *92*, 9083–9100, doi:10.1029/JB092iB09p09083.

Kamb, B. (1991), Rheological nonlinearity and flow instability in the deforming bed mechanism of ice stream motion, *J. Geophys. Res.*, *96*, 16,585–16,595, doi:10.1029/91JB00946.

Kamb, B. (2001), Basal zone of the West Antarctic ice streams and its role in lubrication of their rapid motion, in *The West Antarctic Ice Sheet: Behavior and Environment*, *Antarct. Res. Ser.*, vol. 77, edited by R. B. Alley and R. A. Bindschadler, pp. 157–200, AGU, Washington, D. C.

MacAyeal, D. R. (1989), Large-scale ice flow over a viscous basal sediment: Theory and application to Ice Stream B, Antarctica, *J. Geophys. Res.*, *94*, 4071–4087, doi:10.1029/JB094iB04p04071.

Marshall, S. J. (2005), Recent advance in understanding ice dynamics, *Earth Planet. Sci. Lett.*, *240*, 191–204, doi:10.1016/j.epsl.2005.08.016.

Mayewski, P. A., L. D. Meeker, M. S. Twickler, S. Whitlow, Q. Yang, W. B. Lyons, and M. Prentice (1997), Major features and forcing of high-latitude northern hemisphere atmospheric circulation using a 110,000-year-long glaciochemical series, *J. Geophys. Res.*, *102*, 26,345–26,366.

Ng, F. S. L. (2000), Couples ice-till deformation near subglacial channels and cavities, *J. Glaciol.*, *46*, 580–598, doi:10.3189/172756500781832756.

Nye, J. F. (1951), The flow of glaciers and ice sheets as a problem in plasticity, *Proc. R. Soc. London, Ser. A*, *207*, 554–572.

Nye, J. F. (1959), The motion of ice sheets and glaciers, *J. Glaciol.*, *3*, 493–507.

Oswald, G. K. A., and S. P. Gogineni (2008), Recovery of subglacial water extent from Greenland radar survey data, *J. Glaciol.*, *54*, 94–106, doi:10.3189/002214308784409107.

Pattyn, F. (2002), Transient glacier response with a higher-order numerical ice-flow model, *J. Glaciol.*, *48*, 467–477, doi:10.3189/172756502781831278.

Raymond, C. F., et al. (2001), Ice stream shear margins, in *The West Antarctic Ice Sheet: Behavior and Environment*, *Antarct. Res. Ser.*, vol. 77, edited by R. B. Alley and R. A. Bindschadler, pp. 137–156, AGU, Washington, D. C.

Reusch, D., and T. J. Hughes (2003), Surface "waves" on Byrd Glacier, *Antarct. Sci.*, *15*, 547–555, doi:10.1017/S0954102003001664.

Robin, G. (1958), Glaciology III: Seismic shooting and related investigations, *Sci. Results Norw. Br. Swed. Antarct. Exped. 1949–1952*, *5*, 111–125.

Schoof, C. (2007), Ice sheet grounding line dynamics: Steady states, stability, and hysteresis, *J. Geophys. Res.*, *112*, F03S28, doi:10.1029/2006JF000664.

Siegert, M. J., et al. (1996), An inventory of Antarctic subglacial lakes, *Antarct. Sci.*, *8*, 281–286, doi:10.1017/S0954102096000405.

Thomas, R. H. (1973a), The creep of ice shelves: Theory, *J. Glaciol.*, *12*, 45–53.

Thomas, R. H. (1973b), The creep of ice shelves: Interpretation of observed behaviour, *J. Glaciol.*, *12*, 55–70.

Thomas, R. H. (2004), Force-perturbation analysis of recent thinning and acceleration of Jakobshavns Isbrae, Greenland, *J. Glaciol.*, *50*, 57–66.

Thomas, R. H., et al. (2004), Force-perturbation analysis of Pine Island Glacier, Antarctica, suggests cause for recent acceleration, *Ann. Glaciol.*, *39*, 133–138, doi:10.3189/172756404781814429.

Tulaczyk, S., W. B. Kamb, and H. F. Engelhardt (2000a), Basal mechanics of Ice Stream B, West Antarctica: 1. Till mechanics, *J. Geophys. Res.*, *105*, 463–481, doi:10.1029/1999JB900329.

Tulaczyk, S., W. B. Kamb, and H. F. Engelhardt (2000b), Basal mechanics of Ice Stream B, West Antarctica: 2. Undrained plastic bed model, *J. Geophys. Res.*, *105*, 483–494, doi:10.1029/1999JB900328.

Vance, K., and S. Ashley (2006), Calculating the floating fraction of basal ice along Byrd Glacier, Antarctica, using only the force balance, paper presented at the 13th Annual Workshop of the West Antarctic Ice Sheet Initiative (WAIS), Natl. Sci. Found., Eatonville, Wash.

Van der Veen, C. J. (1999), *Fundamentals of Glacier Dynamics*, 462 pp., A. A. Balkema, Rotterdam, Netherlands.

Weertman, J. (1957a), Deformation of floating ice shelves, *J. Glaciol.*, *3*, 38–42.

Weertman, J. (1957b), On the sliding of glaciers, *J. Glaciol.*, *3*, 33–38.

Weertman, J. (1972), General theory water flow at the base of a glacier or ice sheet, *Rev. Geophys.*, *10*, 287–333, doi:10.1029/RG010i001p00287.

Weertman, J., and G. E. Birchfield (1982), Subglacial water flow under ice streams and West Antarctic ice sheet stability, *Ann. Glaciol.*, *3*, 316–320.

T. Hughes, Department of Earth Sciences, Climate Change Institute, University of Maine, 5790 Edward T. Bryand Global Science Center, Room 223, Orono, ME 04469-5790, USA. (terry.hughes@maine.edu)